UNIVERSITY OF READING

Department of Meteorology

Tropical Cyclogenesis under Radiative-Convective Equilibrium with Background Rotation

Sung-Ho LEE

A dissertation submitted in partial fulfilment of the requirement for the degree of MSc Atmosphere, Ocean and Climate

17th August 2022

Abstract

This study performs 3D cloud-resolving simulations of radiative-convective equilibrium (RCE) under background rotation, with fixed sea surface temperatures (SSTs) near thresholds for tropical cyclone (TC) generation. TCs are allowed to evolve from homogeneous initial conditions. A mid-tropospheric vortex forms preceding the formation of the surface cyclone, coherent with previous observational and modelling studies. The physical mechanisms of TC genesis are analyzed using a variance budget equation for the column-integrated frozen moist static energy (FMSE), adopted from previous approaches in modelling convective self-aggregation using non-rotating RCE simulations. During cyclogenesis and intensification, surface enthalpy feedback dominates over radiative feedback processes, which is significantly stronger compared to other rotating RCE studies. Longwave radiative flux is relatively weaker than reported in the literature. Sensitivity experiments are also performed to determine the dependence of TC genesis on SST, domain size and the presence of a prescribed mean wind. No clear trend was found between warming oceans and intensities of TCs, as well as various feedback processes towards cyclogenesis. The enlargement of the domain prevents the formation of an upper-level cyclone as seen in the control simulations, which lowered the importance of surface fluxes while emphasizing longwave radiative feedbacks, also leading to higher consistency to the literature. Meanwhile, the addition of a mean wind across the troposphere does not cause significant impacts on top of a larger domain. The analysis framework adopted in this study provides a new approach to compare the response of radiative-convective processes during TC genesis across different SSTs and model configurations.

Acknowledgements

First and foremost, I could not have undertaken my MSc course and this dissertation without God, my father in heaven. Also, this endeavor would not have been possible without the invaluable feedback and patience from my supervisors, Prof. Chris Holloway, Prof. Bob Plant and Dr. Jian-feng Gu, especially in reviewing my work and running simulations for this project.

I am also grateful to my classmates from this cohort, for their editing help, entertainment, and emotional support. Lastly, I would be remiss in not mentioning my family and my girlfriend in Hong Kong, my hometown. Their unlimited support and encouragement have kept my motivation high during this process, especially during my stay on the other side of the globe.

Table of Contents

1 Introduction

Despite extensive research on TCs over the past few decades, the mechanisms responsible for the genesis of TCs still lacked scientific understanding. There is general agreement among literature that the spin-up of TCs are facilitated by the pre-existence of mid-level disturbances (Nolan 2007; Davis 2015; Wang et al. 2019; Carstens and Wing 2020), but the processes leading to the subsequent intensification of the surface cyclone remained unclear.

In order to investigate the formation of the precursor and the succeeding cyclogenesis process, idealized model simulations using homogeneous initial soundings were attempted in various studies. In recent years, with the advancement of numerical simulations, it is possible to implement three-dimensional cloud-resolving models (CRMs), at spatial resolutions of up to tens of meters, to simulate tropical convection and understand their dynamics. In particular, a number of studies have made use of radiative-convective equilibrium (RCE) models. RCE refers to the balance between heating of the atmosphere by convection and cooling through radiation in the absence of latent energy transport (Wing et al. 2017, 2018). It is one of the simplest representations of the tropical climate system, which allows the exploration of climate dynamics and sensitivity (Wing et al. 2018). Despite such equilibrium is not observed locally due to the presence of large-scale atmospheric circulations and moisture effects, it could be used as an idealization of the tropical atmosphere over large temporal and spatial scales (Wing and Emanuel 2014). In these experiments, it was widely observed that convective cells organized into clusters spontaneously under homogeneous initial conditions and radiative forcings, namely convective self-aggregation (Wing and Emanuel 2014; Wing et al. 2017, 2018; Pope et al. 2021).

Although the self-aggregating behavior was mainly studied in a non-rotating framework, it was hypothesized that such mechanism is important to TC genesis. With the incorporation of Coriolis parameter into RCE models, namely rotating RCEs, quasi-circular convective clusters formed through self-aggregation were found to organize into TCs in the presence of background rotation (Nolan 2007; Davis 2015; Wing et al. 2016). TCs were generated in models either with prescribed mid-level weak vortex (Murthy and Boos 2018), moist bubble (Wing 2022), or random noise in the temperature field (Davis 2015; Wing et al. 2016; Carstens and Wing 2020). In this study, random perturbations are used in initiating the model, which allows an investigation into the formation of the precursors to the TCs. Following the formation

of the TC, a similar framework for studying convective self-aggregation adopting moist static energy budgets is used for analyzing TC genesis. New to this study is the sensitivity of TC genesis to sea surface temperature (SST), the effect of domain size and the addition of mean wind to the model.

This paper is organized as follows: Section 2 “Literature Review” would be focusing at reviewing existing findings on TC genesis pathways, convective self-aggregation and RCE experiments. Existing findings are summarized while uncertainties could be identified, laying the ground for our research objectives. Section 3 entitled “Methodology” outlines the configurations of numerical models used in the simulations, including physical parameters, domain geometry and resolutions, parameterization schemes and initial conditions. Designs of sensitivity experiments are discussed in detail. The analysis framework on convective-radiative feedback processes, such as frozen moist static energy (FMSE) variance and its budget terms are introduced. Section 4 “Results and Analysis” presents an overview of the simulations, such as evolution of different variables and basic model statistics. Analysis on FMSE variance and convective-radiative feedbacks, followed by a detailed breakdown of individual budget terms, is given. Section 5 outlines notable differences in the behavior of TC genesis in the sensitivity tests compared to the primary simulations discussed in Section 4. The last section summarizes the key results, implications, and potential areas of research in the future.

2 Literature Review

In this section, findings from various literature are summarized. Convective self-aggregation in non-rotating RCE simulations is first discussed, with an emphasis on studies utilizing a FMSE variance budget framework, to be introduced below. Focus is then switched to tropical cyclogenesis in RCEs with background rotation in section 2.2. Research questions are then proposed by the end of this section.

2.1 Convective Self-aggregation

Convective self-aggregation is a process discovered in idealized RCE simulations (Pope et al. 2021). Given homogeneous initial conditions with randomly distributed thermal noise, convection is generated in numerical simulations, and spontaneously aggregate into one or several clusters under certain conditions (Wing and Emanuel 2014; Wing et al. 2017, 2018; Muller and Romps 2018). This results in a quasi-equilibrium state where an intensive moist convective region is surrounded by a broad region of extremely dry, subsiding air devoid of convection (Bretherton et al. 2005; Nolan 2007; Wing and Emanuel 2014; Wing et al. 2020). Over the past two decades, convective self-aggregation has been proven robust across models with various scales, from global climate models (GCMs) to CRMs, and is sensitive to model environmental factors such as SST and domain geometry (Muller and Romps 2018).

However, due to the idealized environment required for self-aggregation to occur, some would argue its relevance to the real world. In particular, the absence of rotation and disturbances such as atmospheric waves in RCE experiments makes its applicability questionable (Muller and Romps 2018). In the real world, the organization of tropical convection occurs in the form of squall lines and quasi-linear clusters in sheared environments (Davis 2015). Weakly sheared environment favors the organization of convection, with TCs as one of the most coherent forms (Davis 2015).

2.1.1 Evolution of Self-aggregation

The evolution of self-aggregation usually initiates with the growth of dry regions, which merge afterwards causing the confinement of moist regions (Wing and Emanuel 2014; Coppin and Bony 2015; Pope et al. 2021). The dry regions then surround the area of most intense convection and strengthen until reaching a quasi-equilibrium state. At the final stage, the organization of convection takes multiple forms in various studies, such as a single

concentrated, moist convective region (e.g., Bretherton et al. 2005; Muller and Held 2012; Wing and Emanuel 2014) and alternating bands of clear, dry regions and moist, convective areas (e.g., Wing et al. 2020; Pope et al. 2021), depending on the initial conditions and model settings.

The organization of convection can be captured by a number of variables. For example, Wing and Emanuel (2014) observed a sharp increase in outgoing longwave radiation (OLR) when convection is increasingly aggregated, and plateaus when a quasi-equilibrium state has been reached. Similar trends were observed for column relative humidity (CRH) and precipitable water (PW). The duration taken to reach aggregation also varied largely across different literature, as well as within different ensemble members of the same studies. This is owing to the highly stochastic nature of self-aggregation, where its evolution is highly dependent on the randomly generated initial conditions (Wing and Emanuel 2014; Wing et al. 2017, 2018).

2.1.2 Physical Mechanisms

In order to identify the key processes contributing to the development of self-aggregation, multiple studies have been carried out utilizing diagnostic frameworks and mechanism denial experiments (Wing et al. 2017). Diagnostic frameworks involved the usage of various metrics to measure the degree of self-aggregation and quantify different contributing processes, while mechanism denial experiments disallow certain processes to test their relative importance to self-aggregation. The following section reviews the physical mechanisms leading to convective self-aggregation in RCE studies, and summarizes results from studies using both approaches.

To measure and quantify the strength of self-aggregation, one of the diagnostic metrics used is the variance of column-integrated frozen moist static energy (FMSE), which differs from the conventional definition of moist static energy (MSE) by the inclusion of a freezing term (equation (1), section 3.2.2) (Bretherton et al. 2005; Wing and Emanuel 2014). Since the freezing and melting of water occurs naturally in clouds, the inclusion of these latent energy terms into the definition of FMSE allows its conservation in adiabatic cloud processes. Wing & Emanuel (2014) further derived a budget equation for FMSE variance, quantifying the contributions of different processes as sources or sinks to the variance, including longwave radiative fluxes, shortwave radiative fluxes, surface enthalpy fluxes and advection (equation (3), section 3.2.2) (Wing and Emanuel 2014; Wing et al. 2017). FMSE variance is closely tied

to the distribution of column PW, since the horizontal variability in temperature is small, while the latent heat term contributes to most of the changes. With an increasing degree of self-aggregation, the convective zone becomes increasingly moist, surrounded by dry regions void of convection. As a result, self-aggregation is associated with an increase in the spatial variance of PW and thus FMSE. In the following part, the physical mechanisms behind the interactions between radiation, moisture, clouds, surface fluxes and advection processes, and their contributions towards convective self-aggregation, would be discussed in detail.

Longwave Radiation

The heating of the atmosphere through longwave radiation is determined by the difference between the fluxes into and out of the atmosphere. Since a fixed homogenous SST is usually implemented at the surface in idealized RCE simulations, the upwelling surface longwave radiation is spatially and temporally constant (Wing and Emanuel 2014). Hence, the column longwave radiative is affected by the outgoing longwave radiation (OLR) at the top of atmosphere (TOA) and downward flux towards the surface, dependent on the amount of water vapour and clouds in the profile. Overall, net longwave radiative flux into the atmosphere is always negative. The presence of optically thick clouds could increase the amount of longwave radiation absorbed, while high clouds with low cloud top temperatures could reduce OLR by the Stefan-Boltzmann law (Pope et al., 2021). Therefore, deep convective clouds often greatly reduce longwave cooling.

Figure 2.1a shows the anomalous longwave and shortwave heating rates of various cloud types in a study on self-aggregation using idealized RCE simulations (anomalies are derived from the domain-averaged values). It illustrates the strong correlation between cloud and longwave heating anomalies. Positive longwave radiative heating anomalies from the horizontal mean are associated with increasing amounts of high clouds and deep clouds during self-aggregation. Meanwhile, low clouds with warm cloud tops and bases foster longwave cooling through strong emission, hence the anomalously low longwave radiative heating rates (Pope et al. 2021).

The primary mechanism of longwave heating on self-aggregation is the direct diabatic effect. Longwave radiative cooling at the dry and clear-sky regions is enhanced, while reduced at moist, cloudy regions, leading to an increase in the domain FMSE variance (Wing et al. 2017). Self-aggregation is also reinforced by the secondary dynamical response to longwave radiative

cooling. Strong cooling at low cloud and dry regions drives subsidence, which generates near-surface outflow and cloud-top inflow by continuity, causing an upgradient transport of FMSE into moist, high-energy regions (Davis 2015; Wing et al. 2017; Muller and Romps 2018). The subsidence also suppresses convection at dry regions while energy is exported. This positive feedback generates further subsidence hence the low-level circulations, sustaining the self-aggregation process.

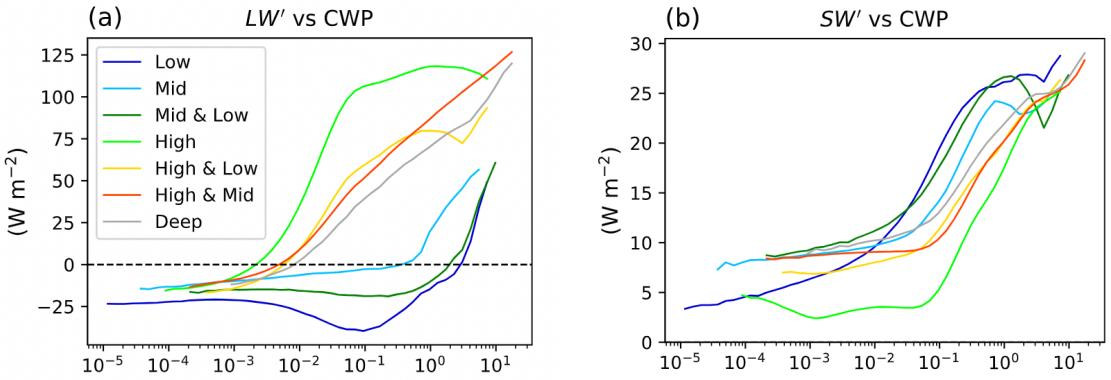

Figure 2.1 - (a) Longwave and (b) shortwave radiative heating anomalies versus condensed water path (CWP) for different cloud types. Statistics obtained from the 300K simulation at mature phase, using UK Met Office Unified Model with an elongated domain (6,048 x 432 km). Reprinted from Pope et al. (2021).

There is broad agreement among literature that longwave radiative feedback is essential towards the occurrence of self-aggregation in non-rotating RCE simulations. In several idealized simulations, strong radiative cooling occurred at the dry regions at early stages, causing a positive longwave radiative feedback and growth of the dry patch (Wing and Emanuel 2014; Holloway and Woolnough 2016; Wing and Cronin 2016; Muller and Romps 2018; Pope et al. 2021). However, there exist some controversy on whether water vapor or clouds is responsible for this process. Wing and Emanuel (2014) argued that this is due to decreased upper tropospheric water vapor, enhancing longwave cooling in the lower troposphere. Meanwhile, multiple studies indicated that the longwave radiative effect mainly came from cloud contributions throughout the simulations (Holloway and Woolnough 2016; Wing and Cronin 2016; Pope et al. 2021), which might be sensitive to the choice of radiation scheme (Wing and Cronin 2016; Wing et al. 2017).

Once the cluster is formed, the longwave feedback is strongly positive at the moist region, since low cloud top temperatures and high opacity of deep convective clouds strongly reduces longwave cooling (Wing and Emanuel 2014; Holloway and Woolnough 2016; Wing and

Cronin 2016; Pope et al. 2021). At the dry region, Wing and Emanuel (2014) saw a transition of the longwave feedback from positive to negative, as the drying up of lower levels reduces longwave. Despite the relative importance of the opposing effects might cause differences in the domain-mean longwave feedback among various simulations, it is certain that strong cloud-longwave effect contributes significantly towards the maintenance of the moist aggregate.

These findings were also supported by mechanism denial experiments. Muller and Held (2012) found that self-aggregation was entirely prevented by homogenizing longwave radiative cooling horizontally at each time step and each height. Their results were robust across a range of domain sizes and horizontal resolutions, which were further confirmed by Arnold and Putman (2018). Similarly, by fixing the radiative cooling with a prescribed value obtained from a smaller domain RCE simulation preceding the main run, Holloway and Woolnough (2016) found that simulations showed a low degree of aggregation. Some form of horizontal organization still occurred, but the moist region was not as confined as in runs with interactive radiative cooling. However, disagreements exist on the relative contribution from different cloud types. Through separating the contributions from low clouds, high clouds and water vapor, Muller and Held (2012) found that turning off the interactive longwave radiation from low clouds (represented by liquid condensates) completely prevented self-aggregation. This was contrasted by Arnold and Putman (2018), who found that longwave cooling by liquid clouds have less effect on aggregation, while removing the ice cloud effects greatly reduced the capability of forming a compact cluster.

Shortwave Radiation

Solar radiation is the major source of shortwave radiation into the atmosphere (Pope et al. 2021). The absorption of shortwave radiation is mainly dependent on the opacity of the atmosphere to these wavelengths. In the troposphere, water vapor is the major atmospheric constituent responsible for the absorption of shortwave radiation, hence the column water vapor path is almost solely responsible for the total shortwave heating rates in the troposphere (Pope et al. 2021). With this regard, there is a strong relationship between FMSE and shortwave radiative fluxes, as FMSE is highly tied to variations in water vapor. As a result, the correlation between FMSE and shortwave radiative flux anomalies is almost positive everywhere in RCE simulations (Wing and Emanuel 2014; Arnold and Putman 2018; Pope et al. 2021).

Meanwhile, clouds are both good absorbers and reflectors of shortwave radiation. Apart from direct shortwave absorption by cloud water, cloud droplets in low clouds act to increase the amount of diffused and reflected radiation, increasing the amount of shortwave radiation absorbed by water vapor (Wing and Cronin 2016). However, high and deeps clouds reflect shortwave radiation at upper levels, reducing the amount of radiation reaching the troposphere. Therefore, atmospheric heating rates depend on cloud types, illustrated in Figure 2.1b. For example, high clouds generally have the lowest shortwave heating rates (Pope et al. 2021) (Note that Figure 2.1b shows the combined vapor and cloud shortwave radiative heating anomalies). The effect of clouds could be either positive or negative on shortwave atmospheric heating, but would still produce an overall positive feedback when combined with the moisture effect in most cases (Wing and Cronin 2016; Wing et al. 2017; Pope et al. 2021).

Similar to longwave radiative feedback, the effect of shortwave feedback on self-aggregation could be partitioned into the direct diabatic effect and the dynamical response. If only the former is considered, most current studies suggested that shortwave radiative feedback has a small, positive contribution towards the early stages of self-aggregation, but not essential towards the FMSE variance budget (Wing and Emanuel 2014). At mature stage, shortwave feedbacks are found to be important in maintaining the mature aggregated state (Wing and Emanuel 2014; Holloway and Woolnough 2016). This is mainly due to the increased absorption of shortwave radiation by water vapor at moist, high-FMSE regions compared to the dry regions (Wing and Emanuel 2014). Further decomposition of the direct diabatic effect revealed that all-sky and clear-sky components of shortwave flux were of similar levels, confirming that water vapor absorption dominates over cloud modulations in the shortwave feedback budget (Wing and Emanuel 2014; Holloway and Woolnough 2016). In contrast, Muller and Held (2012) found that shortwave feedback prevents self-aggregation at earlier stages of simulation. Holloway and Woolnough (2016) argued that it should be an effect of the dynamical response. When both mechanisms are considered, the effect of forced circulation dominates over the diabatic effect, hence weakly inhibiting self-aggregation (Holloway and Woolnough 2016; Wing et al. 2017).

Similarly, importance of shortwave feedback towards self-aggregation could be assessed by denial experiments. By removing interactive shortwave radiative feedback, Muller and Held (2012) observed self-aggregation in their simulations across a range of domain sizes and

resolutions, indicating that shortwave inhomogeneities are not crucial for self-aggregation to occur.

Surface Enthalpy Flux

Surface enthalpy flux is the sum of sensible and latent energy flux near the surface. It arises from the thermodynamic disequilibrium between the ocean and the atmosphere immediately above it, as well as the variations in surface wind speed (Wing and Emanuel 2014). The former refers to the enhanced evaporation and heat transfer due to the differences in moisture and temperature respectively, known as the air-sea enthalpy disequilibrium. The latter is described as the wind-induced surface heat exchange (WISHE) effect, owing to enhanced sensible and latent heat flux in the presence of wind (Wing and Emanuel 2014). The air-sea disequilibrium feedback is larger at dry regions than in the moist regions, which leads to enhanced surface fluxes at the former but suppressed at the latter, creating a negative feedback towards self-aggregation (Wing et al. 2017). Meanwhile, the WISHE effect counteracts the disequilibrium feedback. Stronger surface winds in moist, intense convective regions due to convective gustiness enhance surface enthalpy fluxes, creating a positive feedback (Muller and Held 2012; Wing and Emanuel 2014; Wing et al. 2017). The relative importance of these opposing effects determines the sign of the surface flux feedback at different stages of aggregation.

In non-rotating RCE simulations, it is widely agreed among literature that surface flux feedbacks are strong, positive contributors to early stages self-aggregation (Muller and Held 2012; Wing and Emanuel 2014; Wing and Cronin 2016; Pope et al. 2021). The WISHE effect dominates over the air-sea disequilibrium effect initially, creating a net positive surface flux feedback (Wing et al. 2017). One exception is Pope et al. (2021) who found that surface flux feedback was strongly negative initially, but detailed investigation was not provided. During the maintenance stage, the importance of the surface flux feedback declines (Wing and Cronin 2016), or even dampens aggregation in some studies (Wing and Emanuel 2014; Pope et al. 2021). This is due to the increased amount of moisture within the moist region with aggregation, causing an anomalously weak air-sea disequilibrium effect, hence a negative surface flux feedback.

Multiple denial experiments have been made in the past to investigate the necessity of surface flux feedback towards self-aggregation. Bretherton et al. (2005) found that simulations with

horizontally homogenized surface fluxes did not aggregate. Muller and Held (2012) extended the sensitivity experiments to a range of horizontal resolution and domain size, concluding that self-aggregation could still occur without interactive surface fluxes. They argued that given interactive radiative feedbacks, with larger domains or coarser resolutions, convection could aggregate without surface fluxes. Meanwhile, Holloway & Woolnough (2016) found that convective cells lacked horizontal structure with uniformly prescribed surface fluxes, while the degree of aggregation was also dependent on the strength of surface fluxes imposed on the model. It could be said that surface flux feedbacks are important towards the initiation of self-aggregation, but are not sufficient to support aggregation without longwave radiative feedbacks (Wing et al. 2017).

Advective Processes

Advective processes refer to the transport of FMSE by the circulation. From equation (10), the advective term describes the spatial covariance between the column divergence of FMSE and FMSE itself. This term tracks the regions corresponding to FMSE import and export (Wing and Emanuel 2014; Carstens and Wing 2022). Part of the advective term is the dynamical response to diabatic heating in various parts of the domain, as described above. In most studies, the sum of all advective processes was a strong negative feedback at most stages of aggregation, exporting FMSE from moist, high energy regions (e.g., Wing and Cronin 2016; Pope et al. 2021). In some simulations, advective processes were found to be positively contributing to self-aggregation at the intermediate stages (Bretherton et al. 2005; Wing and Emanuel 2014; Holloway and Woolnough 2016), which involves shallow circulations driven by low-level radiative cooling. However, large controversies existed in the sign and magnitude of the advective feedback among different simulations.

Despite the sign of the domain-averaged advective feedback is negative, local upgradient transport of FMSE could still be present, but counteracted by other stronger advective processes (Holloway and Woolnough 2016; Wing et al. 2017). As such, some studies attempted to isolate the dynamical response through analyzing the shallow circulations and effective stream-functions to assess their importance. However, these are beyond the scope of this study and would not be discussed further.

2.1.3 Sensitivity to Sea Surface Temperature

Over the past decade, convective self-aggregation was widely studied with various model setups, parameterizations, and radiative transfer schemes, as well as its sensitivity to environmental factors like sea surface temperature (SST). For example, the RCE model intercomparison project assessed the robustness of self-aggregation over a wide range of models of different resolutions, as well as its climate sensitivity (Wing et al., 2018). The following section discusses previous findings related to the dependence of self-aggregation on SST in non-rotating RCE studies. Although this study mainly focuses on tropical cyclogenesis in a rotating RCE framework, its processes are comparable to self-aggregation in some aspects, therefore might share similar mechanisms responsible for the dependence on SST.

Convective self-aggregation is highly sensitive to SST, both in terms of intensity and the ability to aggregate. A number of studies pointed out that simulations at low SSTs failed to aggregate, roughly below a threshold of 300 K (Khairoutdinov and Emanuel 2010; Wing and Emanuel 2014). Self-aggregation was still observed in some studies at much lower SSTs like 280 K (Wing and Cronin 2016), while some failed to aggregate at high SSTs (Wing and Emanuel 2014), both possibly due to the domain geometry adopted in the simulations. Meanwhile, simulations with higher SST were also found to reach a higher degree of aggregation at the steady state (Wing and Cronin 2016).

The dependence of aggregation on SST was investigated by analyzing the sensitivity of individual feedback processes. Wing and Cronin (2016) found that the longwave feedback is negative at cooler SSTs at early stages of aggregation, which transitioned into a strong positive term in warmer runs, agreeing with Emanuel et al. (2014). However, controversies existed for its mechanisms. Wing and Cronin (2016) hypothesized that at cooler SSTs, the atmosphere is optically thin that any presence of clouds would enhance radiative cooling by increasing the emissivity of the atmosphere, causing a stronger negative feedback. Pope et al. (2021) confirmed this hypothesis by a detailed analysis on contributions from individual cloud types. This contrasted with Emanuel et al. (2014), who proposed that it should be a clear-sky effect, where water vapor instead of clouds caused the enhanced cooling effect.

The shortwave feedback is found to be always positive, and decreases with SST in a number of studies (Wing and Cronin 2016; Wing et al. 2017; Pope et al. 2021), despite its cause is still

debated. Wing and Cronin (2016) found that this trend is associated with a declining cloud contribution with warmer SSTs. Pope et al. (2021) argued that this is a vapor effect. While column water vapor increases with SST exponentially, column shortwave heating increases with column water vapor logarithmically, leading to a linear positive trend. However, the range of FMSE values also increases exponentially with SST. Upon normalization by the range of FMSE to remove the dependence on SST (equation (11)), the shortwave feedback decreases with warming oceans. Wing et al. (2017) suggested that the relative importance of clear-sky and cloud effects might be sensitive to the choice of model and radiative schemes.

The sensitivity of surface fluxes to SST is relatively unclear. While Wing and Cronin (2016) found that surface flux feedback is similar across SSTs, Pope et al. (2021) reported a less negative feedback with warmer runs at the mature stage. Meanwhile, GCM simulations by Coppin and Bony (2015) showed that higher SSTs yielded stronger surface winds, hence stronger surface flux feedback. However, it is worth noting that all idealized studies imposed a fixed SST, might not be representative of the real atmosphere as air-sea interactions were absent (Wing et al. 2017).

2.2 Tropical Cyclogenesis

The discussion above main focused on the mechanisms responsible for convective self-aggregation in non-rotating RCE simulations. With the incorporation of sufficient background rotation in RCEs, self-aggregation of convective clusters takes the form of TC genesis spontaneously (Bretherton et al. 2005; Nolan 2007; Khairoutdinov and Emanuel 2013; Davis 2015; Wing et al. 2016, 2017; Muller and Romps 2018; Wang et al. 2019; Carstens and Wing 2020; Ruppert et al. 2020; Carstens and Wing 2022). The physical mechanisms of spontaneous TC genesis were found to be similar to convective self-aggregation, at least at the early stages (Wing et al. 2016). This section first summarizes the pathway leading to the genesis of TCs, and the relevance to idealized models like rotating RCE simulations. The physical mechanisms behind these processes are then discussed in 2.2.2.

2.2.1 Genesis Pathway

Considering the formation of TCs, it was generally agreed among literature that the development of a strong near-surface cyclone was preceded by a mid-tropospheric mesoscale moist vortex (Nolan 2007; Davis 2015). The mid-level cyclonic vorticity was believed to be associated with a strong increase in vertical mass flux with height at low levels, which created a horizontal mass convergence in the boundary layer (Wang et al. 2019). This then created a small-scale vortex at the surface, which subsequently became the core of an intensifying TC (Nolan 2007).

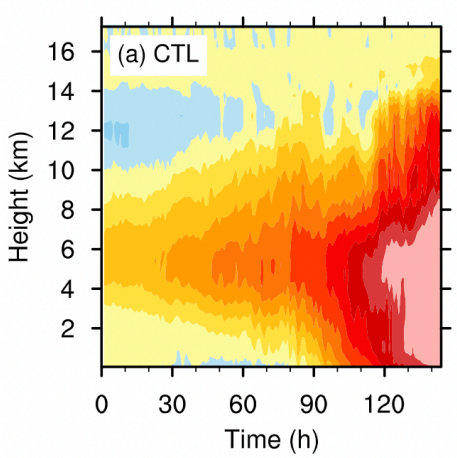

Figure 2.2 - Vortex-following Hovmöller diagrams of vertical area-mean relative vorticity (10^{-5} s^{-1}), averaged over a 150 x 150km box centered on the vortex at 6km. Reprinted from Fig. 3 in Wang et al. (2019)

In a number of idealized simulations, a coherent vortex was observed to form at mid-troposphere, which subsequently develop into a TC on the time scale of a few days (Davis 2015; Wang et al. 2019; Carstens and Wing 2020). Wang et al. (2019) observed the movement of a strong cyclonic vortex from mid-troposphere (z = 4 - 8km) towards the surface by tracking vortex centers at multiple height levels (Figure 2.2), consistent to the set of high-*f* simulations done by Carstens and Wing (2020). Relative vorticity values at lower levels were found to sharply increase following a steady intensification of the mid-level vorticity (Davis 2015; Wang et al. 2019).

Differences existed in the evolution of the mid-tropospheric vortex among different rotating RCE simulations. Some studies observed the formation of a single large moist cluster, following the expansion of the dry region similar to self-aggregation, which then started rotating and eventually develop into a TC (Wing et al. 2016). Another pathway was the merging of multiple moist vortices into a single cyclone, which then dried up the surroundings (Davis 2015).

2.2.2 Physical Mechanisms

Various approaches have been used in studying the physical mechanisms leading to TC genesis in rotating RCE simulations. While a number of studies focused on the detailed dynamic and thermodynamic evolution of the antecedent mid-tropospheric vortex (Nolan 2007; Davis 2015; Wang et al. 2019), some explored the origin of these coherent vortical structures in the context of self-aggregation (Bretherton et al. 2005; Nolan et al. 2007; Wing et al. 2016). While convective self-aggregation is believed to provide a framework for studying the genesis of TCs, there still exist a gap on whether similar radiative-convective feedbacks are responsible for TC genesis.

Similar to convective self-aggregation, the spatial variance of FMSE was found to be increasing with enhanced degree of organization of the moist, convective regions. The consistency between self-aggregation and the TC genesis motivates the use of the same framework in quantifying the mechanisms responsible for TC genesis (Wing et al. 2016; Muller and Romps 2018; Carstens and Wing 2022). In the following part, the roles of each of the feedback processes in rotating RCE simulations are discussed. However, there is currently a limited number of studies utilizing FMSE variance budgets to study TC genesis, therefore large uncertainties exist within these findings, which also paves the way for the objectives of this study.

Longwave Radiative Feedback

Longwave radiative feedback was one of the major processes that dominated the early stages of TC genesis, similar to the initial development of non-rotating simulations (Wing et al. 2016; Muller and Romps 2018). Carstens and Wing (2022) argued that the importance of longwave feedbacks was dependent on the Coriolis parameter chosen for the study, where the longwave term was dominant in low-*f* simulations at early stages, but less significant in high-*f* settings. Following maturity of the TC, the contribution from longwave radiation increased and continued as the second most significant term following surface enthalpy fluxes (Wing et al. 2016; Muller and Romps 2018; Carstens and Wing 2022)

A majority of studies found that the longwave feedback was mainly a cloud effect at the moist region throughout the simulations (Davis 2015; Wing et al. 2016; Ruppert et al. 2020; Carstens and Wing 2022), caused by the ‘cloud greenhouse effect’ described by Ruppert et al. (2020).

This effect was trapping of longwave radiation by deep convective clouds with high emissivity, similar to the process described in section 2.1.2. In addition to the cloud effects, Ruppert et al. (2020) observed a clear-sky contribution from strong low-level radiative cooling in the dry regions at early stages, which was similar to the expansion of the dry region in non-rotating self-aggregation (Wing and Emanuel 2014).

Mechanism denial experiments suggested that longwave radiative feedback was not strictly necessary for TC genesis, but could possibly delay its formation when interactive radiative feedback was eliminated (Wing et al. 2016; Muller and Romps 2018). Muller and Romps (2018) found that simulations with interactive longwave feedback accelerated TC genesis by a factor of 2 compared to those without. This contrasted with non-rotating RCEs, where homogenizing longwave cooling rates mostly prevented self-aggregation, or at least greatly reduced the level of aggregation. With this regard, Wing et al. (2016) argued that while TC genesis in rotating RCE shared similar processes with non-rotating self-aggregation, convective organization was more robust in rotating simulations.

Shortwave Radiative Feedback

Similar to self-aggregation, at early stages there was consensus that shortwave radiative feedback had a weakly positive contribution to tropical cyclogenesis. Later in the simulations, Carstens and Wing (2022) found that shortwave feedback became one of the major contributors to FMSE variance in low-f environments, similar to non-rotating simulations (Wing and Emanuel 2014; Wing and Cronin 2016; Wing et al. 2016). This shortwave effect was mainly a clear-sky effect as described in section 2.1.2. However, this contribution decreased as f increased, agreeing with other studies using higher f values. Muller and Romps (2018) found that homogenizing shortwave radiation in their simulations had relatively little impact on TC genesis, further confirming that shortwave radiative flux was not crucial to TC formation.

Surface Enthalpy Feedback

Traditionally, the primary source for TCs was latent heat flux through evaporation over the ocean surface (Riehl 1950). TCs were believed to intensify through WISHE feedback, following the formation of an initial surface vortex (Emanuel 1986). This was consistent with observations where TCs preferentially develop over areas with significant potential for heat fluxes, and decay over land due to the absence of evaporative flux (Zhang and Emanuel 2016).

In idealized studies of TC genesis using rotating RCE simulations, surface enthalpy flux was one of the strongest sources of FMSE variance growth (Wing et al. 2016; Muller and Romps 2018; Ruppert et al. 2020; Carstens and Wing 2022), despite there existed some controversy on whether surface flux is the sole leading term. Upon maturity of the TC, there was a wide consensus that surface flux being the major leading order feedback (Wing et al. 2016; Muller and Romps 2018; Carstens and Wing 2022), consistent with existing TC theories. This contrasted non-rotating aggregation where it became a negative feedback once a mature cluster formed (Wing and Emanuel 2014; Pope et al. 2021). Wing et al. (2016) argued that this difference was due to much stronger winds in the moist region associated with the rapidly intensifying cyclone, leading to an enhanced WISHE feedback, dominating over the air-sea disequilibrium effect.

The importance of surface enthalpy flux to tropical cyclogenesis was again assessed by mechanism denial experiments in various studies. Muller and Romps (2018) found that if surface fluxes are homogenized horizontally, a weak TC could still form but could not reach its full intensity, agreeing with Murthy and Boos (2018). This was also consistent with Zhang and Emanuel (2016), who reported the development of the TC was greatly inhibited when a capping wind speed was imposed on the surface flux scheme. The same study also applied the same limit in simulating a real-life storm, which yielded a much weaker storm compared to the actual category-3 hurricane. With this regard, Murthy and Boos (2018) argued that surface enthalpy fluxes were more important for the intensification of the TC than the initial development of circulation.

Advective Processes

There is wide agreement among rotating RCE studies that the advection term in the FMSE variance budget was negative throughout the simulations (Wing et al. 2016; Muller and Romps 2018; Carstens and Wing 2022). That means the circulation transported moist static energy from moist, high-energy regions to dry, low-energy regions, damping the growth in FMSE variance (Wing et al. 2016). This contrasted non-rotating aggregation where the advection transported FMSE upgradient, facilitating self-aggregation of the convective cluster (Muller and Held 2012; Wing and Emanuel 2014). Carstens and Wing (2022) argued that the sign of advective feedback was dependent on the strength of background rotation. They observed that the advective feedback is more negative with increasing f values, due to stronger divergence of

high MSE from moist regions at upper levels. In high-*f* settings, the strong surface flux feedback overcomes advection, whilst in medium-*f* runs weaker surface fluxes could barely balance the negative advective feedback, which slows or even prevents self-aggregation.

Due to the fact that TC genesis is entirely diabatically driven (Wing et al. 2016), and that the advective term is calculated as the residual of the variance tendency which includes multiple processes within, detailed examination on this term is beyond the scope of this study.

2.2.3 Sensitivity to Sea Surface Temperature

The response of TC formation under global warming has been a subject of considerable investigation, both in the form of observational studies and climate projections. Various attempts have been made to analyze and project the change in frequency and intensity of TCs in a warming climate, but conflicting results and large uncertainties existed (Knutson et al. 2010). The following section summarizes major findings on the sensitivity of TCs to warming SSTs.

Despite effort in analyzing the sensitivity of TC activities and intensities to warming SSTs from observations, it remains a difficult task to test the response of TC under warming global oceans given the relatively short reliable historical records, compared to the time span where effect from climate forcings becomes apparent (Ramsay et al. 2020). Projections by global climate models are yet to be verified for the same reason. Therefore, an alternative approach would be implementing idealized high-resolution models like rotating RCEs to study TC variability under a warming scenario. However, the domain size of this type of simulations typically only allowed a single TC to form using Earth-like tropical parameters (Ramsay et al. 2020). Some studies attempted to increase the number of TCs by artificially increasing the Coriolis parameter (nicknamed “TC World”) (Khairoutdinov and Emanuel 2013; Chavas and Reed 2019), but the number is still highly restricted by the inter-cyclone spacing and the competition for available moisture. Together with the lack of loss mechanism for TCs to dissipate, such as the depletion of moisture flux into the TC following landfall, the ability of idealized models in measuring the response of TC frequency is questionable (Ramsay et al. 2020). Ramsay et al. (2020) attempted to relate the time for a vortex to reach a certain threshold from a weak initial strength (incubation period) to the propensity for TC formation hence its frequency, but more work is required to prove its relevance to the real world.

Regarding the dependence of TC intensity on SST, previous studies usually linked TC properties to variables like potential intensity (PI) and Coriolis parameter instead of SST, as SST is not a fundamental controlling variable to TC, and surface energy balance is absent with the specification of a uniform SST (Emanuel 1987; Chavas 2013; Khairoutdinov and Emanuel 2013). Khairoutdinov and Emanuel (2013) observed an increase in TC size, intensity, and precipitation rates with SST, following the increase of PI. TCs tended to deepen more (in terms of minimum surface pressure) at warmer SSTs, while velocities scaled with PI, agreeing with previous studies (Held and Zhao 2008; Chavas 2013). Ramsay et al. (2020) also reported a linear increase in PI with SST, and an enhanced maximum TC intensification rate with warming. Their simulations suggested that TC intensification rates might exceed existing prediction based on PI (e.g., Emanuel 2012). However, the thermodynamic factor leading to such change is uncertain. Predicting and explaining TC intensification rates at warming SSTs remains a challenge with our current understandings to TC theories.

2.3 Research Objectives

In this study, the mechanisms leading to TC genesis in rotating RCE simulations is investigated by addressing the following questions:

- What is the genesis pathway of TC? Does a mid-level disturbance precede the intensification of a surface cyclone?

If a pre-TC mid-level vortex forms in the simulations, it is believed to resemble real world cyclogenesis processes, and therefore could facilitate understanding on TC genesis mechanisms. We then inquire the followings:

- What are the dominant cloud-radiative feedback processes during tropical cyclogenesis, and how do they differ from non-rotating RCE simulations?
- Is the evolution of cyclogenesis sensitive to initial conditions such as SSTs, the presence of mean wind and domain geometry? If so, what are the possible mechanisms responsible for such change?

A similar framework for studying convective self-aggregation is adopted in analyzing tropical cyclogenesis, using moist static energy variance budget. New to this field is the sensitivity of tropical cyclogenesis to various sea surface temperatures (SSTs), as well as the effect of domain geometry and the addition of mean wind to the model. We also introduce the use of a normalized FMSE budget by Pope et al. (2021), which serves as a novel systematic approach in analyzing spontaneous TC genesis under varying SSTs in idealized simulations.

3 Methodology

This section describes the methodology adopted in this study. Section 3.1 first summarizes the detailed model settings in our rotating RCE simulations, followed by the design of various sensitivity experiments. The framework for analyzing the physical mechanisms of TC genesis is then described in section 3.2.

3.1 Simulation Design

3.1.1 Model Setup

The spontaneous genesis of TC under RCE with rotation is simulated with a three-dimensional, non-hydrostatic, non-linear, time-dependent and fully compressible model — Cloud Model 1 (CM1) (Bryan and Fritsch 2002). CM1 has been extensively used for idealized studies of atmospheric phenomena, including understanding RCE, rotating RCE and the dynamics of TCs in both axisymmetric and three-dimensional geometry (e.g., Davis 2015; Wang et al. 2019).

A simple Smagorinsky-like scheme for turbulence is used to parameterize the planetary boundary layer. The horizontal eddy viscosity depends on a horizontal length scale l_h, which is a function of surface pressure ($l_h = 100$ m for surface level pressure of 1015 hPa and increases linearly to $l_h = 1000$ m for 900 hPa) (Bryan 2012). Cloud microphysics is parameterized with the Morrison double-moment scheme (Morrison et al. 2005, 2009). Surface fluxes are calculated using simple bulk aerodynamic formulation. The surface drag coefficient c_d is based on Fairall et al. (2003) at low wind speed and Donelan et al. (2004) at high wind speed. The surface exchange coefficient for enthalpy c_k is fixed at 1.2×10^{-3} (Drennan et al. 2007). The Rapid Radiative Transfer Model (RRTM) is used as the shortwave and longwave scheme (Mlawer et al. 1997; Clough et al. 2005; Iacono et al. 2008).

A square domain is employed with doubly periodic boundary conditions on an f-plane, with lengths of 1,080 km in both zonal and meridional directions and a horizontal resolution of 3 km. This domain geometry is comparable to prior studies utilizing rotating RCEs simulating TC genesis, ranging roughly between 750and 2,000 km, and was shown to facilitate self-aggregation and subsequent TC genesis. The model has 64 vertical levels, with the lowest model level at 25 m and model top at 28 km. The vertical grid spacing is 50 m near the surface, which gradually stretches to 500 m above 5 km. To reduce the influence of reflected of gravity waves, Newtonian damping is applied toward base state as a sponge layer above 20 km.

The lower boundary is a uniform ocean surface with a constant sea surface temperature (SST). The SST setting is varied across the set of simulations to assess the sensitivity of TC genesis in rotating RCE. More details are provided in Section 3.1.2. The Coriolis parameter f is set to $5 \times 10^{-5} s^{-1}$, approximately corresponding to the value at 20° latitude. Most previous studies modelling TC genesis with rotating RCEs adopted this value. It was also shown to support TC formation consistently among a range of tropical f-plane values (Carstens and Wing 2020). The incoming solar radiation is spatially uniform and constant in time, with a solar constant of 650.83 W m^{-2} and a fixed zenith angle of 50.05 W m^{-2}. These yield an insolation of 417.9 W m^{-2}, similar to Bretherton et al. (2005).

In order to investigate the natural process of TC genesis as one of the objectives of this study, the model is allowed to develop organized circulations spontaneously from a homogeneous environment, instead of implementing a pre-existing moist bubble or mid-level vortex. This allows us to observe the genesis pathway of the TC in our simulations. The initial sounding is taken from the mean profile of the final 30 days of a non-rotating RCE simulation in a smaller square domain (108 km) at the same resolution, initialized with random perturbations in the temperature field at the lowest 5 model levels. The amplitude of the perturbation decreases linearly from the maximum 0.1 K at the lowest level to zero at the 6th level.

3.1.2 Sensitivity Experiments

Several sensitivity experiments are performed in this project. Firstly, SST is altered across the set of simulations. Constant SSTs are chosen in the range between 298K to 301K at 1K intervals. The range of SSTs roughly correspond to 26℃, the temperature above which TC formation is possible in the current climate (Palmen 1948; Gray 1968, 1977), despite spontaneous TC genesis was shown to be possible at much lower SSTs of 285K and 295K in rotating RCE simulations (Wing and Emanuel 2014; Wing et al. 2016). Similar sensitivity experiments have been done on non-rotating RCE simulations (Wing and Emanuel 2014; Wing and Cronin 2016; Wing et al. 2018; Pope et al. 2021). Wing et al. (2016) mentioned that rotating RCE simulations exhibited similar behavior across different SSTs qualitatively, but a comprehensive study on TC genesis and relevant cloud-radiative feedbacks have not been done so far. The dependence of convective aggregation on SST, in particular with background rotation, is therefore one of the main themes to be investigated in this project.

Model domain is the second variable to be modified in the sensitivity tests. A square domain of sides 2304 km is employed with the same horizontal resolutions, at 301K SST (1080 km and 2304 km simulations are referred to as 'g0360' and 'g0768' in the figures). In the set of 1080 km simulations across all SSTs, an upper-level cyclone forms at the 'antipode' of the surface cyclone quickly after genesis, which extends to the surface while interacting with the first cyclone, killing it and replacing with a new cyclone at the antipodal point (see Section 4 for detailed discussion). We hypothesize that such effect is purely artificial, possibly related to the convergence of outflow air at the opposite side of the domain. With such regard, the domain size is altered to test the robustness of such phenomenon. If the anomaly is sensitive to domain geometry, the interference of the upper-level cyclone to the development of the TC could then be minimized by altering the domain size.

The third sensitivity test performed is the addition of mean wind. In a number of non-rotating and rotating RCE studies, a minimum wind speed is seen by the surface flux scheme in order to account for the unresolved turbulence in the boundary layer (Naumann et al. 2017; Murthy and Boos 2018; Mol et al. 2019) (More details are discussed in 5.3). Due to a technical issue in compiling the model, this threshold is absent in our simulations. The model might be highly unstable to any winds due to abnormally low surface fluxes in this wind-limiting regime, and is possibly one of the causes of the upper-level cyclone. Therefore, a mean wind of 3 ms^{-1} is added to one of the simulations with 2304 km domain. The resultant difference is then analyzed to examine the effect of such numerical subtlety.

3.2 Analysis Framework

3.2.1 Genesis Timing

The timing of cyclogenesis is defined as the first time when the maximum tangential wind speed at the lowest model level reaches tropical storm strength (34 kt, ~17.5 ms^{-1}) (National Hurricane Center and Central Pacific Hurricane Center, n.d.), and continues to increase in the next model output time step, following the approach in Carstens and Wing (2022). The tangential and radial wind components are computed by interpolating the wind speed at the lowest model level (25 m) from the center of the TC, defined by the location of minimum surface pressure. This definition is similar to previous studies (e.g., Wing and Cronin 2016; Carstens and Wing 2020), but slightly modified due to the coarser model output frequency.

Tropical storm strength is adopted instead of hurricane strength (64 kt) in order to identify the timing before TCs intensifies rapidly, instead of reaching maturity.

3.2.2 Frozen Moist Static Energy (FMSE) Variance and Budget

To quantify the importance of convective-radiative feedback in the generation and development of TCs, column-integrated frozen moist static energy (FMSE) is invoked in this study, as discussed in section 2.1.2. FMSE is the sum of sensible heat, latent heat and potential energy of an air parcel, defined by equation (1):

$$h = c_p T + gz + L_v q - L_f q_{c,i} \tag{1}$$

where c_p is the specific heat capacity of dry air, L_v is the latent heat of vaporization, L_f is the latent heat of fusion, q is the water vapor mixing ratio, and $q_{c,i}$ is the condensed ice water mixing ratio. Density-weighed vertical integral of FMSE $(\hat{h})$ is then computed.

$$\hat{h} = \int_0^{TOA} \rho(z) h(z) dz \tag{2}$$

The density-weighted vertical integral of FMSE is conserved during moist adiabatic processes, including melting and freezing of precipitation, as well as convection (Wing and Emanuel 2014; Wing et al. 2016). It is only affected by radiation, surface fluxes and advection of column integrated FMSE. With this regard, a budget equation for $\hat{h}$ could be derived:

$$\frac{d\hat{h}}{dt} = SEF + NetSW + NetLW - \nabla_h \cdot \widehat{\vec{u}h} \tag{3}$$

where NetSW and NetLW are the column shortwave and longwave radiative flux convergences, SEF is the surface enthalpy flux, and the last term is the advection of $\hat{h}$. The surface enthalpy flux term is defined as the sum of sensible and latent heat fluxes:

$$SEF = SHF + LHF \tag{4}$$

$$SHF = \rho c_H c_p U(T_s - T_a) = \rho c_H c_p U \Delta T \tag{5}$$

$$LHF = \rho c_E L_v U\left(q^*_{T_s} - q_v\right) = \rho c_E L_v U \Delta q \tag{6}$$

where ρ is the density of air at the lowest model level, c_H and c_E are the sensible heat and latent heat exchange coefficients, U is the surface wind speed, T_s is the surface temperature, T_a is the near-surface air temperature, $q^*_{T_s}$ is the saturation water vapor mixing ratio at the surface temperature, and q_v is the near-surface water vapor mixing ratio. Sensible and latent heat fluxes are computed as part of the model output and directly utilized for following analysis. However, for the decomposition of SEF into its components, equations (5) and (6) are necessary.

$$NetSW = NetSW_{top} - NetSW_{bottom} \tag{7}$$

$$NetLW = NetLW_{top} - NetLW_{bottom} \tag{8}$$

The shortwave and longwave convergence terms refer to the net amount of radiation entering the column. These are given by the difference between the net downward radiative flux at the top of atmosphere (TOA) and the bottom of the atmosphere.

$$\begin{aligned} SEF' = {} & \rho L_v (c_E U)' \{\Delta q\} + \rho c_p (c_H U)' \{\Delta T\} + \rho L_v \{c_E U\} (\Delta q)' + \rho c_p \{c_H U\} (\Delta T)' \\ & + \rho L_v (c_E U)' (\Delta q)' + \rho c_p (c_H U)' (\Delta T)' - \rho L_v \{(c_E U)' (\Delta q)'\} - \rho c_p \{(c_H U)' (\Delta T)'\} \end{aligned} \tag{9}$$

Surface enthalpy fluxes are mainly due to the thermodynamic disequilibrium between the ocean surface and the overlying atmosphere, and the transfer of energy owing to surface wind speed variations. Hence it would be intuitive to partition the surface flux feedback term into these respective components. Equation (9) shows the decomposed surface flux anomalies: the first two terms are the variations solely due to surface wind speed (U), or the WISHE effect; the following two terms are the variations solely due to air-sea disequilibrium (ΔT and Δq); and the remaining is the eddy term representing the covariance of the two. Wing and Emanuel (2014) showed that the variations in surface exchange coefficients c_E and c_H correlate strongly with the wind speed but not with the disequilibrium terms, therefore could be combined with the wind speed in calculating anomalies in equation (9).

The relative importance of different physical processes to self-aggregation, quantified by the spatial variance of column integrated FMSE, is analyzed using budget equation (10), derived by Wing and Emanuel (2014).

$$\frac{1}{2}\frac{dvar(\hat{h})}{dt} = \{\widehat{h'SEF'}\} + \{\widehat{h'NetSW'}\} + \{\widehat{h'NetLW'}\} + \{\widehat{h'\nabla_h \cdot \vec{u}h}\} \quad (10)$$

The four terms on the right hand side of budget equation (10) are the surface enthalpy flux term, shortwave term, longwave term and the advective term respectively. Bracketed terms ($\{X\}$) denote the horizontal mean of the variables, while primed terms (X') denote anomalies from its instantaneous domain mean. All terms are the domain-averaged correlation between the anomalies of the terms in equation (3) and the anomaly of column integrated FMSE. These are calculated from the instantaneous output from the model, except the advective term which is calculated as a residual from the rest of the budget, following Wing et al. (2016) and Pope et al. (2021), owing to difficulties in closing the budget with the infrequent model outputs available.

The variance of $\hat{h}'$ increases with the degree of convective organization, as moist regions become moister and dry regions become dryer (Muller and Romps 2018). In the budget equation, a positive covariance between $\hat{h}'$ and the diabatic sources represents an anomalous source of FMSE in a region of high FMSE with respect to the domain mean, or an anomalous sink of FMSE in a low FMSE region (Wing and Emanuel 2014). Both processes lead to a positive tendency in the spatial variance of $\hat{h}'$, which are commonly referred to as positive feedback mechanisms on convective aggregation and cyclogenesis, amplifying the incipient storm (Wing et al. 2016; Ruppert et al. 2020).

3.2.3 Normalization of FMSE

In order to compare the column integrated FMSE budgets across simulations with different SSTs, normalization of FMSE variance and the budget terms is necessary due to the strong dependence of FMSE on temperature. The Clausius-Clapeyron equation suggests an exponential relationship between temperature and saturation vapor pressure in the atmosphere, increasing the amount of water vapor held by a warmer atmosphere. This causes a significant change in FMSE due to contribution from latent energy. To eliminate such dependence on SST, this study follows the approach taken by Pope et al. (2021), normalizing vertically integrated FMSE using the theoretical upper and lower limits of FMSE ($\hat{h}_{max}$ and $\hat{h}_{min}$):

$$\hat{h}_n = \frac{\hat{h} - \hat{h}_{min}}{\hat{h}_{max} - \hat{h}_{min}} \quad (11)$$

The lower limit of FMSE ($\hat{h}_{min}$) is defined as the column integrated FMSE of a dry adiabatic profile with zero moisture in the troposphere. Above the troposphere, vertically integrated MSE from the initial sounding is used. For the upper limit, a fully saturated moist pseudo-adiabatic profile is used in the troposphere. Similarly, the initial profile is used above the tropopause. The SST of each simulation is used as the surface temperature initiating the dry and saturated profiles. The tropopause is defined as the lowest level where the lapse rate decreases to 2 K/km or less in the initial profile. The values of the limits and properties of the tropopause are summarized in Table 3.1. Values used in this study are slightly different from figures reported in Pope et al. (2021), due to different initial soundings applied to the model.

SST (K)	*Surface pressure (hPa)*	$\boldsymbol{\theta_{sfc}}$ *(K)*	*Tropopause altitude (km)*	*Tropopause pressure (hPa)*	$\boldsymbol{\hat{h}_{min}}$ *(GJ/m^2)*	$\boldsymbol{\hat{h}_{max}}$ *(GJ/m^2)*	$\boldsymbol{\hat{h}}$ *above tropopause (GJ/m^2)*
298	1010.32	297.13	11.25	215.74	3.247	3.391	0.728
299	1010.64	298.10	11.75	200.66	3.263	3.419	0.681
300	1010.99	299.06	11.75	202.62	3.277	3.449	0.688
301	1011.38	300.03	12.25	188.60	3.294	3.481	0.643

Table 3.1 – Values of $\hat{h}_{max}$ and $\hat{h}_{min}$ used for normalizing column-integrated MSE for each SST

Since the latent heat of vaporization term often dominates over other terms in FMSE, the spatial variability of FMSE is closely related to PW. The normalization of FMSE with the difference between a dry and moist profile was shown to eliminate most of the dependence of $var(\hat{h})$ on SST in non-rotating RCE, with normalized MSEs reaching similar levels at equilibrium state (Pope et al. 2021).

4 Results and Analysis

4.1 Overview

Spontaneous TC genesis is found to occur at all SSTs and all model configurations, matching previous studies using a similar range of SSTs (Wing et al. 2016). The simulations exhibit comparable results qualitatively across all SSTs in the 1080 km domain runs, except differences due to the stochastic nature of convective aggregation. In the following section, the 301K simulation is selected as the control run which most of the discussions is based on. Section 5 provides more detailed analysis on the sensitivity of TC genesis to SST and other environmental parameters in the model.

4.1.1 Outgoing Longwave Radiation

Plan views of instantaneous outgoing longwave radiation (OLR) from day 15 to day 40 at 5-day increments are shown in Figure 4.1. On day 15, patches of randomly spaced small convective cells are present across the domain. The scales of clouds range from a few kilometers to hundreds of kilometers, with various cloud top temperatures indicating the difference in cloud depths. A relatively large band of clouds with cold cloud tops have already developed by this stage, while a large number of small cells with shallower depths are present. By day 20, convective cells have organized into larger patches and cooler cloud tops, while large amounts of randomly spaced small cloud cells are still present. Patches of clear skies are observed. 5 days later, the cloud cells have aggregated into a single large quasi-circular patch with signs of rotation, showing strong convective activity and the possibility of development into a tropical depression. Convection is suppressed away from the main cloud cluster. More vortical motion is observed on day 30. By day 35, the rotating cloud cluster have developed into a mature TC of radius around 200 km, with a clear eye and distinct circular bands of clouds around the core. The TC has further intensified by day 40 with colder cloud tops near the eye wall and a larger eye. Clouds are absent away from the TC following its formation.

The size of the cyclone in our simulation is relatively small compared to mature TCs in the real world. It is mainly controlled by the size of the domain where sufficient space is required for outflow from the top of the TC to subside. When the domain size is increased, a larger TC forms owing to the reduced restriction imposed by the domain boundaries. Also, the choice of Coriolis parameter f possibly affects the Rossby radius of deformation, where higher f yields a smaller TC.

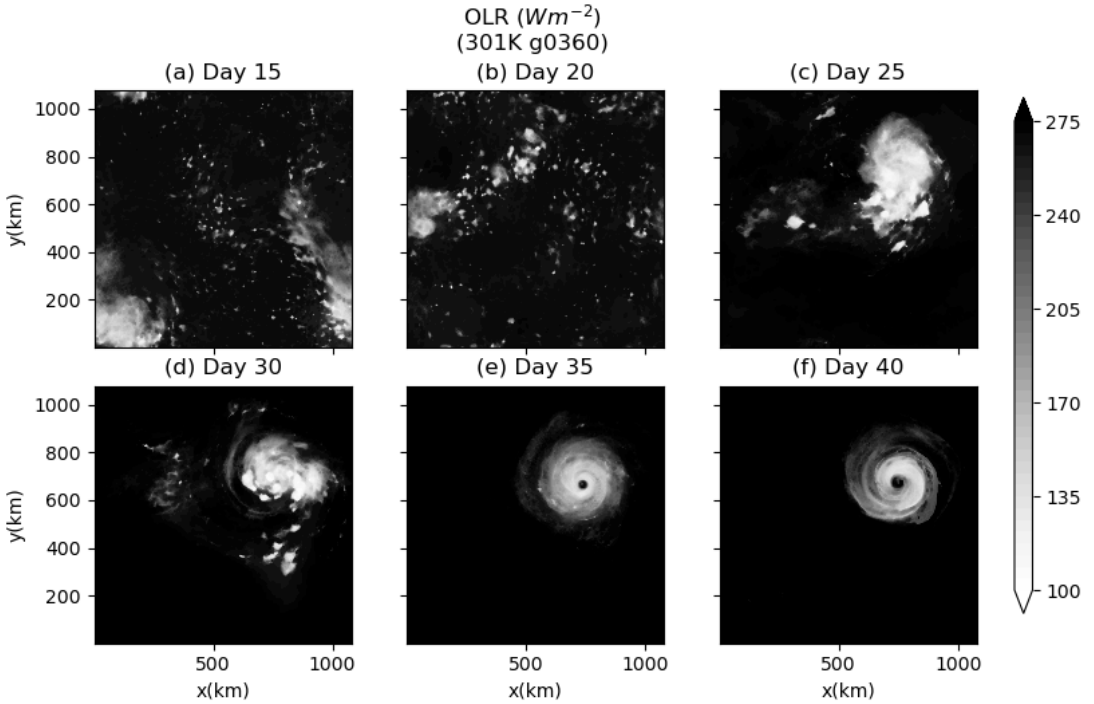

Figure 4.1 – Instantaneous snapshots of outgoing longwave radiation (OLR) (Wm^{-2}) on days (a) 15, (b) 20, (c) 25, (d) 30, (e) 35 and (f) 40 of simulation at 301K in 1080 km domain.

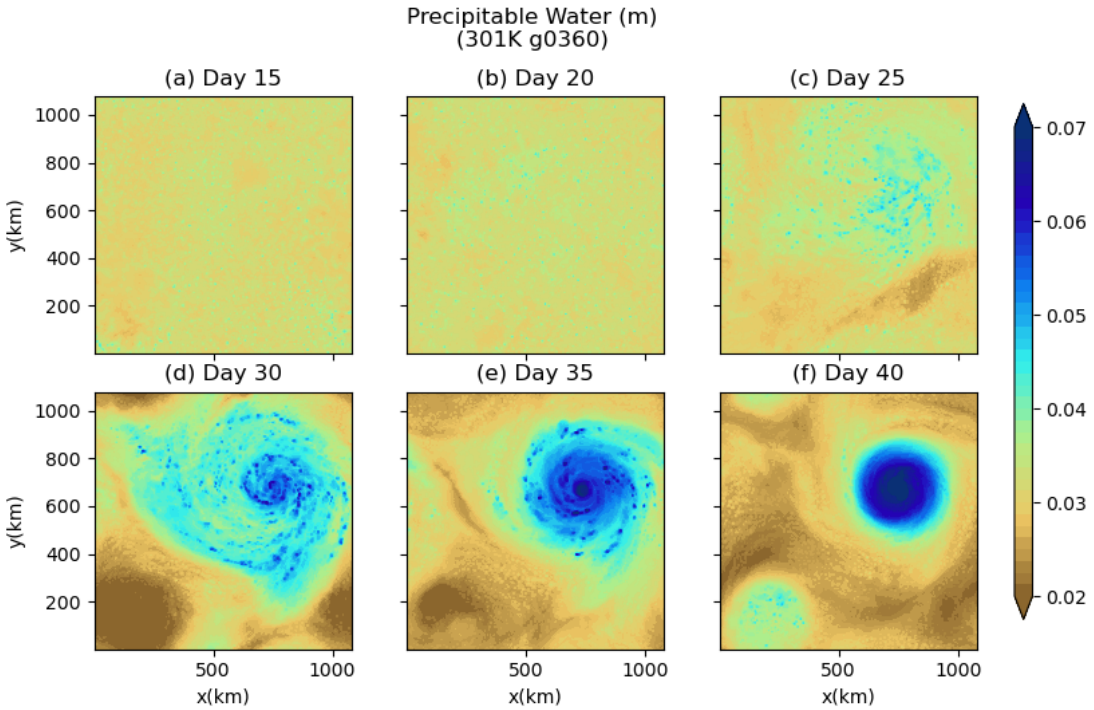

Figure 4.2 – Instantaneous snapshots of precipitable water (m) on days (a) 15, (b) 20, (c) 25, (d) 30, (e) 35 and (f) 40 of simulation at 301K in 1080 km domain.

4.1.2 Precipitable Water

Figure 4.2 shows the snapshots of column PW on the same days as in Figure 4.1. On day 15, the spatial distribution of PW is nearly homogeneous, with randomly spaced moist spots. This corresponds to the randomly distributed spots of convection generated by the initial sounding. More concentrated patches of moist and dry regions emerge by day 20. By day 25, it has further agglomerated into an area of high PW surrounded by dry areas. The moist cluster roughly corresponds to the area of thick clouds (low OLR) in Figure 4.1. On day 30, a circular moist patch is observed with swirling bands of moist air, where no clouds are present in the OLR fields. This feature shows a high degree of convective aggregation with strong vortical motion, which suggests the formation of a TC. At the same time, an extremely dry patch also developed in the opposite side of the domain where convection is suppressed. By day 35, the region of high PW has further contracted around the core of the storm with a maxima near the core, indicating the intensification of the TC. On day 40, the moist patch organizes into a circular patch of highly moist air with radius around 200 km, roughly corresponding to the size of the cloud bands in the OLR field.

Meanwhile, away from the surface cyclone, another circular feature emerges and gradually moistens over time (Figure 4.2c – e). Its location roughly matches the antipodal point of the doubly periodic domain. This corresponds to an upper-level cyclone, possibly due to the convergence of air from TC outflow. More details are discussed in section 4.1.4.

4.1.3 Wind Speed and Timing of TC Genesis

Figure 4.3 displays the Hovmöller diagrams for azimuthal maximum and averaged wind speeds, decomposed into the tangential and radial components from the point of minimum surface level pressure. In Figure 4.3a, a large increase in maximum tangential wind speed is seen at both surface and mid-tropospheric levels on around day 30, which corresponds to the timing of the rapid intensification of the TC. Following the definition of cyclogenesis in section 3.2.1, it successfully captures the timing before the rapid intensification occurs, the period where this study is interested in. In Figure 4.3b, strong cyclonic winds are observed as the TC intensifies, exceeding 40 ms^{-1} on average. Strong inflow of wind is also present in Figure 4.3c, corresponding to the strong surface convergence. Following a peak in maximum surface tangential wind at 75 ms^{-1} before day 35, where the convective cells have organized into a mature cyclone as seen in Figure 4.1, winds weaken and sustain between 40 – 50 ms^{-1}, until

day 60 when the TC dissipates and re-forms after day 80. In order to avoid the interference of the second cyclone, the following analysis is focused on the first 40 – 50 days of the simulations.

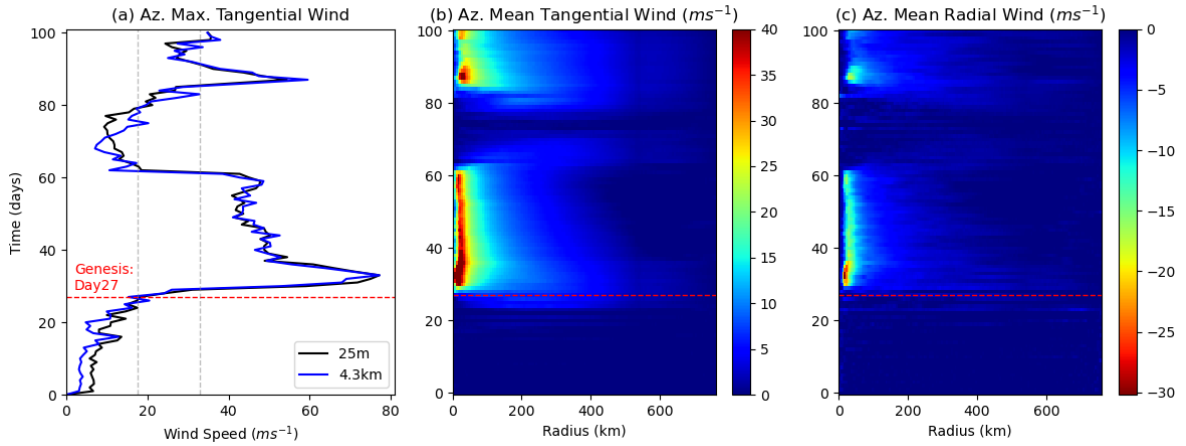

Figure 4.3- Hovmöller diagrams of simulation at 301K in 1080 km domain of (a) azimuthal maximum tangential wind at 25 m and 4.3 km (ms^{-1}); (b) azimuthal mean tangential wind at the lowest model level (ms^{-1}); (c) surface azimuthal mean radial wind at the lowest model level (ms^{-1}). Dashed red lines in all plots represent the timing of TC genesis. Dashed grey lines in (a) indicate wind speeds corresponding to tropical storm strength (34 kt) and hurricane strength (64 kt). Cyclonic tangential winds are defined positive, while radial winds are positive away from the TC center. In (c), the color bar is saturated at 0. All components of winds are interpolated and decomposed with respect to the point of minimum surface level pressure.

4.1.4 Relative Vorticity

Snapshots of relative vorticities at the lowest model level (25 m), mid- and upper-troposphere (4.3 km, 10.3 km) during the early stages of the 301K simulation are shown in Figure 4.4. From the surface plots, spots of positive vorticity evenly distributed across domain, with a background of weakly negative vorticity on day 15. Vorticity patches of both signs gradually merge and become organized as the degree of aggregation increases, with areas of positive vorticity roughly matching with moist, cloudy regions in Figure 4.1 and Figure 4.2. With increasing heights, vorticity patches become increasingly organized. Vorticity patches of opposite signs interlocks each other within convective clusters, where strong contrasts in vorticities exist. Strong band-like positive vorticities are observed at the upper troposphere prior to genesis, which turned into circular bands around the TC alternating with negative bands of vorticity. At mid-levels, a more distinct positive patch existed around the TC, surrounded by weakly negative vorticities.

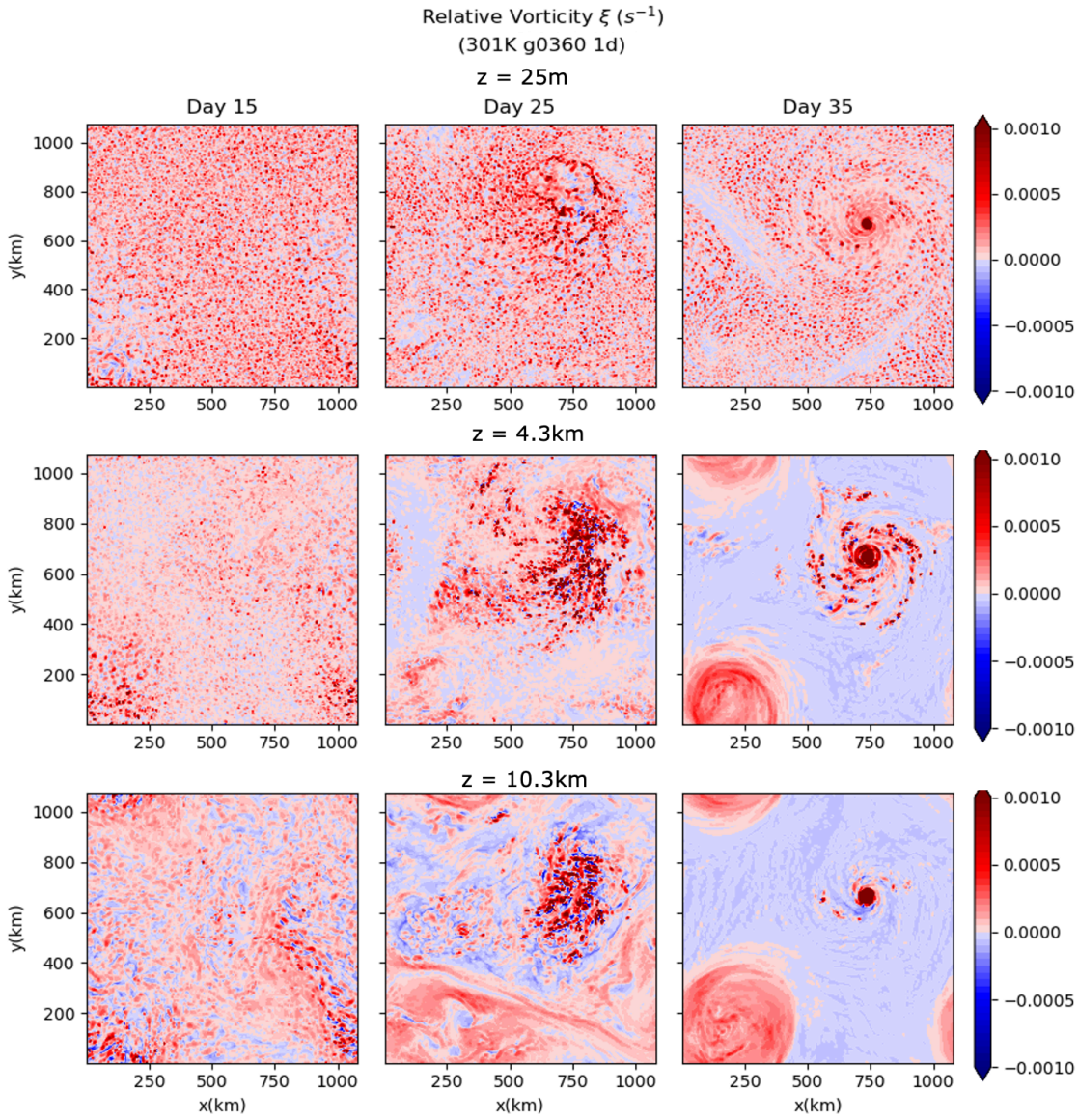

Figure 4.4 – Instantaneous snapshots of relative vorticity (s^{-1}) on days 15, 25 and 35 of simulation at 301K in 1080 km domain, at (a) 25 m; (b) 4.3 km; (c) 10.3 km heights.

As mentioned, an upper-level vortex emerged prior to genesis. On day 35, a moderately strong cyclonic feature with wide circulations is observed at the left-lower corner of the domain. This is hypothesized to be an artificial feature, owing to the convergence of outflowing air from the top of TC at the opposite side of the domain. Initially, this upper-level cyclone is extremely dry (Figure 4.2d), which gradually gains moisture while extending towards the surface, illustrated by the circular patch of moist air in Figure 4.2f. After the surface cyclone reaches maturity, the upper cyclone starts interacting with the TC, drawing moisture and high vorticity air (not shown). Eventually the surface cyclone is replaced by the upper-level vortex, generating a new TC below the upper-level cyclone. The dissipation and formation of a new cyclone is also reflected in the drop and intensification of wind speeds between days 60 and 90 (Figure 4.3).

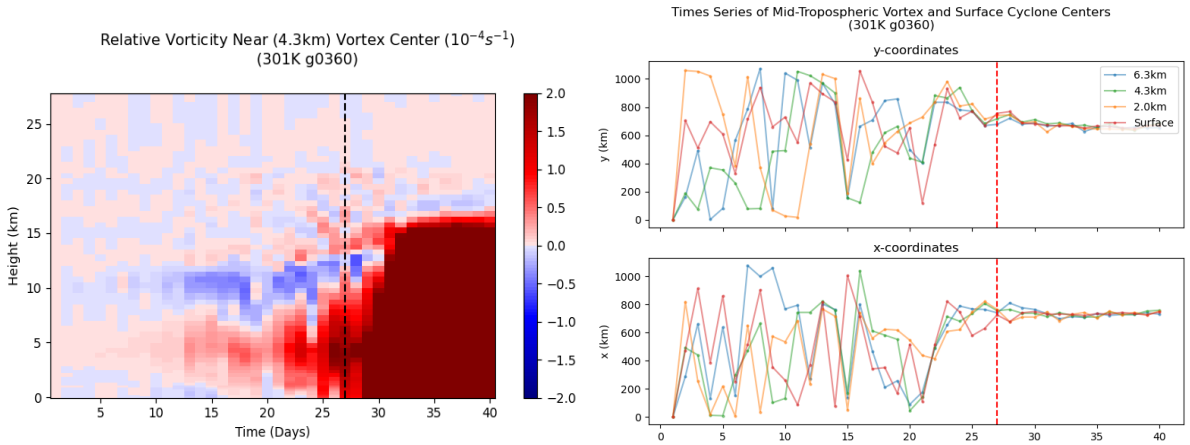

(Left) Figure 4.5 - Hovmöller diagram of daily column relative vorticity (s^{-1}), averaged in a 150 x 150 km box around the 4.3 km height vortex center. Vortex center is tracked by the point of daily maximum relative vorticity smoothed over a 150 x 150 km box.

(Right) Figure 4.6 –Time series of vortex center coordinates at surface, 2.0 km, 4.3 km, and 6.3 km heights. All vortex centers follow the same definition in Figure 4.5, except for the surface which is defined as the point of minimum surface pressure. Vertical dotted lines represent the genesis time. Both diagrams taken from simulation at 301K in 1080 km domain.

However, it is difficult to identify the genesis pathway of the cyclone through these plots. To verify the emergence of a mid-level vortex observed by Carstens and Wing (2020) and Wang et al (2019), the mid-tropospheric vortex is tracked by identifying the daily maxima in the relative vorticity field at 4.3 km height, smoothed over a 150 km x 150 km box. The Hovmöller diagram of the column relative vorticity at the vortex center is plotted in Figure 4.6a. The time-height plot depicts the formation of a mid-tropospheric vortex preceding the intensification of the surface cyclone. A maxima in relative vorticity emerged roughly 15 days before genesis at 5km height, with an anticyclonic outflow above. The evolution of relative vorticity largely resembles Wang et al. (2019) and Carstens and Wing (2020), despite they reported a later occurrence of 3-5 days prior to genesis. Afterwards, the mid-level maxima intensifies one day before genesis, followed by the generation of strong cyclonic vorticity in the lower troposphere in the following 2 days. This matches with the rapid strengthening of cyclonic wind speeds in Figure 4.3a. A strong anticyclonic flow exists above 10 km, corresponding to the outflow of the TC. Eventually the vortex extends across the entire troposphere by day 32, accompanied by a weak outflow aloft.

The identification of vortex center might depend on the choice of vertical levels, as noted by Carstens and Wing (2020). The time series of the vorticity center coordinates (Figure 4.6b) reveals that the location of maximum vorticity at 2.0 km, 4.3 km and 6.3 km converges approximately 5 days ahead of genesis, roughly matching with the timing when the mid-level

vortex emerges in simulations by Wang et al. (2019) and Carstens and Wing (2020). Before converging, the location of the tracked center scattered at different parts of the domain. This suggests that the mid-tropospheric peak in vorticity detected up to 15 days ahead of genesis might be due to multiple developing convective regions, before a single coherent vortex forms. Nevertheless, the mid-tropospheric vortex center is located at the same location at least 5 days ahead of cyclogenesis. Qualitatively, the Hovmöller diagrams of column relative vorticities by tracking vortex centers at different levels also resembles the results in Figure 4.6a (see appendix – Figures 7.1 and 7.2). This proves the robustness of our results to the choice of vertical level in tracking the vortex center.

4.2 Physical Mechanisms

In the following section, the physical mechanisms behind cyclogenesis in our rotating RCE simulations is analyzed, following the FMSE variance budget framework described in section 3.2.2.

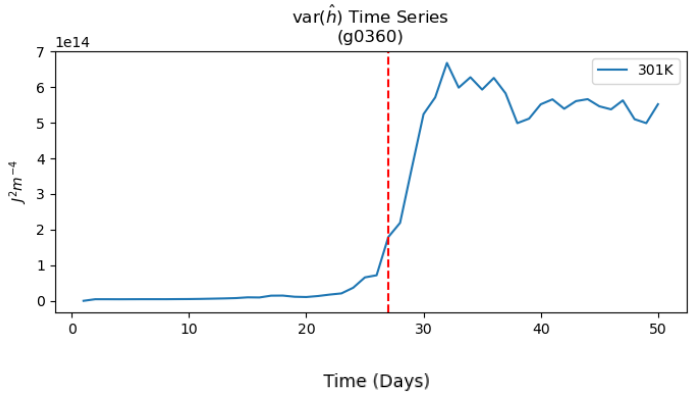

Figure 4.7 – Day 1-50 time series of FMSE variance of simulation at 301K in 1080km domain. Vertical dotted line represents the genesis time.

Figure 4.7 shows the evolution of FMSE variance ($var(\hat{h})$) in the first 50 days of simulation. $var(\hat{h})$ increases sharply around genesis, matching with the increased degree of aggregation of convective systems within the domain. $var(\hat{h})$ plateaus at around $6 \times 10^{-4} J^2 m^{-4}$ during maturity of TC.

As discussed in section 3.2.2, the growth rate of $var(\hat{h})$ is controlled by longwave radiative fluxes, shortwave radiative fluxes, surface enthalpy fluxes and advective processes. Figure 4.8 displays the evolution of the domain-mean of each budget terms in the variance budget. Similar to other rotating RCE experiments (Wing et al. 2016; Muller and Romps 2018), the FMSE

variance budget terms largely resemble a non-rotating RCE simulation at the initial stage. This indicates that the development of convective systems leading to cyclogenesis is similar to self-aggregation. The only difference is during the mature stage, where surface enthalpy flux is the strongest term, while it is a negative feedback in non-rotating simulations.

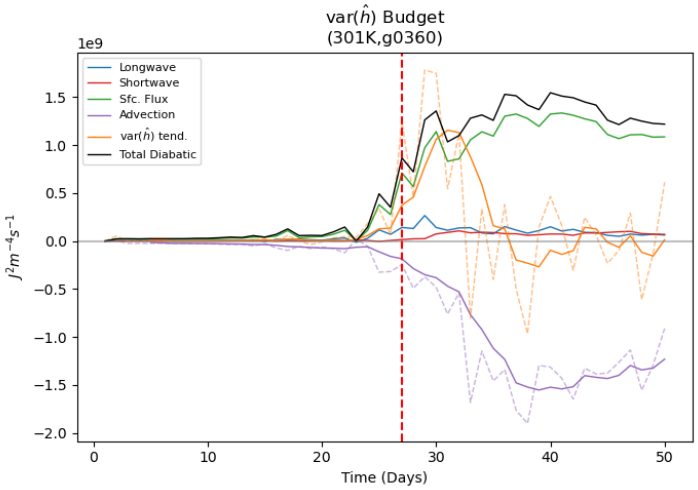

Figure 4.8 – Day 1–50 time series of domain-mean FMSE variance budget terms of simulation at 301K in 1080 km domain. Diabatic terms (longwave flux, shortwave flux, and surface enthalpy flux) are derived and plotted from daily instantaneous model outputs. Solid lines for advection term and $var(\hat{h})$ tendency are 5-day running averaged, while dotted lines show the daily instantaneous values. Vertical dotted line represents the genesis time.

At early stages of the simulation (Days 1-20), the surface enthalpy flux term is the dominant positive contribution towards aggregation. Longwave and shortwave radiative effects are limited, while advection dampens the increase in aggregation. 5 days preceding genesis, a positive $var(\hat{h})$ tendency is observed corresponding to the rise in Figure 4.7. This is accompanied by an increase in the longwave radiative component, roughly corresponds to one-third of surface flux contributions. Shortwave radiative fluxes remain consistently small, while a notable increase in the magnitude of advective term is observed. Following genesis, the surface enthalpy flux dominated over other terms due to the strong wind speeds around the cyclone core through day 50. Coinciding the timing when $var(\hat{h})$ starts to stabilize, the shortwave term increases, contributing approximately equally with the longwave term. The magnitude of the advective term roughly balances the diabatic terms at this stage.

Figure 4.9 shows the spatial distribution of FMSE anomalies (h') on days 10 to 40 at 10-days intervals. Compared to Figure 4.2, regions of high $\hat{h}'$ roughly corresponds to moist areas in the PW field and vice versa. This illustrates the strong positive correlation between $\hat{h}'$ and moisture

as discussed in section 2.1.2. With this regard, the contributions of the budget terms in equation (10) from moist and dry regions could be diagnosed using the $\hat{h}'$ values at each column. Here an approach modified slightly from Wing and Emanuel (2014) is adopted.

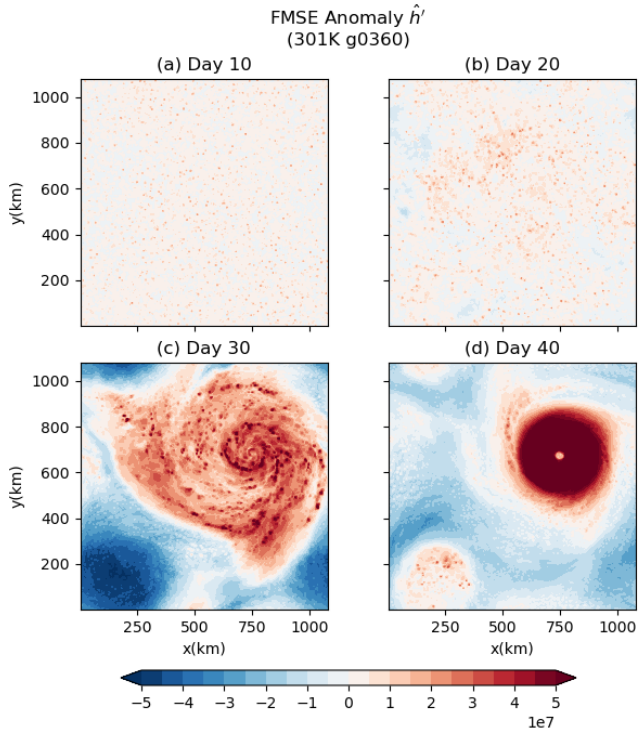

Figure 4.9 – Snapshots of vertically integrated FMSE anomalies on day 10, 20, 30 and 40 of simulation at 301K in 1080km domain.

In Figure 4.10, the variance budget terms are further decomposed. Due to the increase in $var(\hat{h})$ with time, the correlation terms in equation (9) are first normalized by the domain-averaged $var(\hat{h})$ ($\{\hat{h}'\}$) on each day for easier interpretation, especially at early stages when the budget terms are relatively small. The domain is then divided into blocks of 48 x 48 km, within which the values of each budget terms are averaged, compromising between noisiness and avoiding loss of details. The blocks are then sorted according to the block-averaged $\hat{h}'$ in ascending order, with low $\hat{h}'$ on the left and high $\hat{h}'$ on the right, corresponding to dry and moist blocks respectively. This slightly differed from Wing and Emanuel (2014), where they ranked blocks by CRH. Our analysis showed that both approaches gave highly similar results, therefore $\hat{h}'$ is used here for simiplicity. Figure 4.10 below displays the Hovmöller diagrams of block-sorted budget terms in the first 50 days of the 301K simulation, and can be compared with the panels in Wing and Emanuel (2014) (their Figure 6) and Holloway and Woolnough (2016) (their Figure 5 and 6).

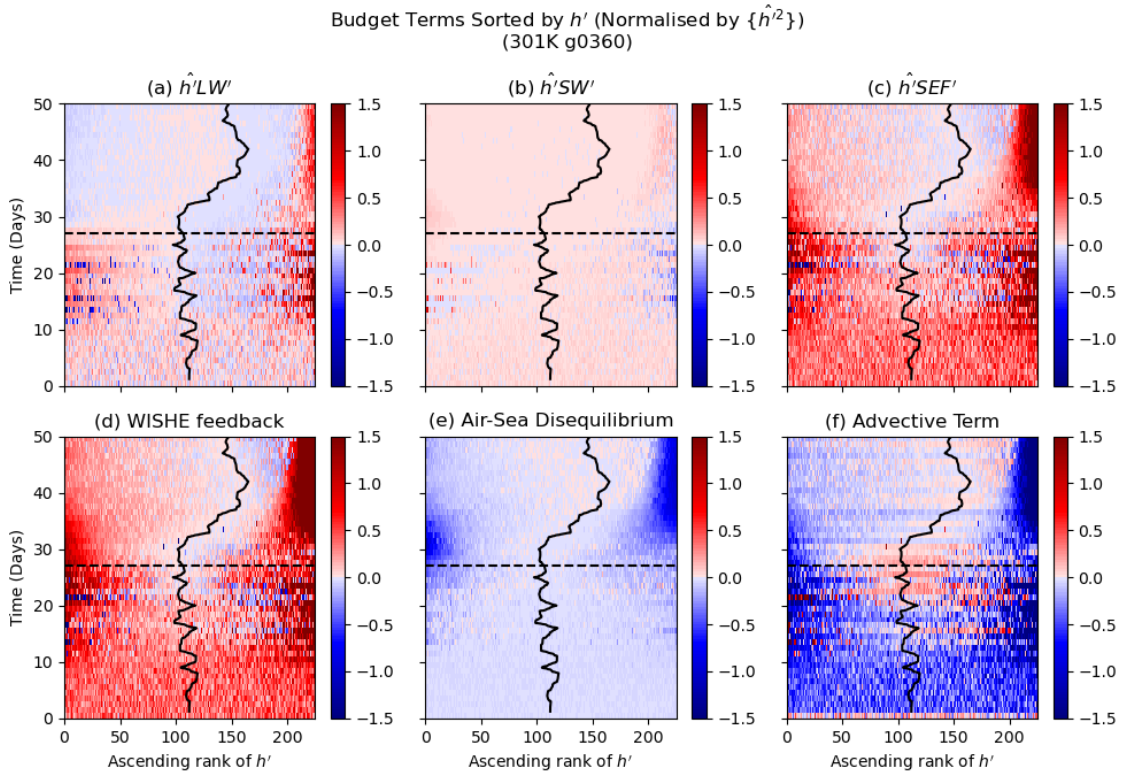

Figure 4.10 – Correlation between vertically integrated FMSE anomalies and anomalies of (a) longwave radiative flux, (b) shortwave radiative flux, (c) surface enthalpy flux, (d) surface enthalpy flux due to wind speed anomalies (WISHE feedback), (e) surface enthalpy flux due to air-sea disequilibrium anomalies, (f) advective term. All terms are averaged by 48 x 48 km blocks and normalized by daily domain-mean $var(\hat{h})$ ($\{\hat{h}'\}$), in units of d^{-1}. Blocks are sorted by h' in ascending order, with dry regions on the left and moist regions on the right. The black solid line is the $\hat{h} = 0$ contour, while dashed horizontal lines represents the genesis time. Values taken from simulation at 301K in 1080 km domain.

In the following section, contributions from each term would be discussed individually. Since tropical cyclogenesis is diabatically driven, discussion would be primarily focused on the three diabatic terms.

Shortwave Feedback

The shortwave radiative feedback is first examined. From Figure 4.10b, it could be seen that the correlation between $\hat{h}'$ and column shortwave convergence is nearly positive everywhere. This matches with most previous studies (e.g., Wing and Emanuel 2014; Arnold and Putman 2018), due to the strong tie between water vapor and shortwave heating rates as discussed in section 2.1.2. Throughout the simulation, most of the shortwave feedback comes from the driest and moistest areas, despite not immediately obvious from Figure 4.10b due to the smaller magnitudes of the shortwave term compared to others. As shortwave heating rates are largely tied to the amount of water vapor in the column, we attempt to explain these features using relative humidity arguments.

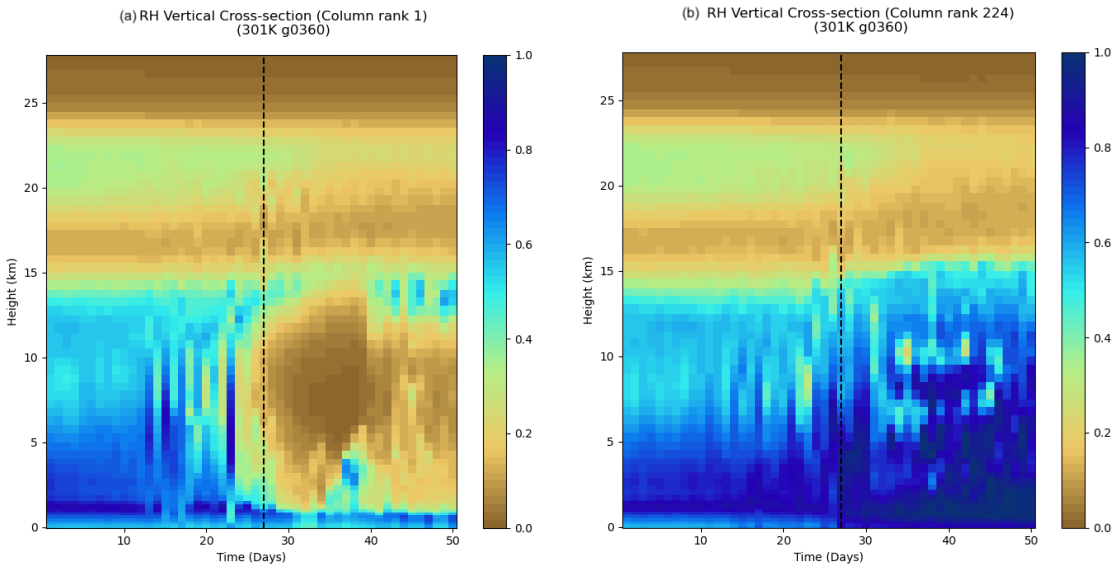

Figure 4.11 – Hovmöller diagrams of daily vertical cross-section of relative humidity averaged over 48 x 48 km blocks, at the (a) lowest (rank 1) and (b) highest (rank 224) column-integrated FMSE anomaly blocks. Values taken from simulation at 301K in 1080 km domain. Black dotted lines represent the genesis time.

At the driest patch (Figure 4.11a), the atmosphere dries up from the mid-troposphere to near-surface levels. The low humidity in the dry patch sustains throughout the mature stage of the cyclone, leading to a reduced absorption of incoming solar radiation, amplifying the dry patch. This process resembles the findings by Wing and Emanuel (2014) and Holloway and Woolnough (2016).

Despite the shortwave feedback is weakly positive across the domain, there are some negative contributions embedded between positive feedbacks within the moistest region before genesis, which was not seen in previous RCE studies with and without background rotation. Figure 4.11b shows high relative humidity throughout the lower troposphere, and around 50% in the upper troposphere during this period, which only explains the positive feedback in the background. Horizontal plots of OLR (not shown) and the shortwave feedback term (Figure 4.12) reveals that areas of negative shortwave feedback roughly corresponds to low OLR values amongst cloudy regions, which might suggest strong reflection of solar radiation by deep clouds. This leads to the reduction of shortwave radiation penetrating into the troposphere hence weaker radiative heating.

Following cyclogenesis, the area of negative feedback has contracted towards the eyewall, surrounded by circular bands of positive shortwave flux both inwards and outwards (Figure 4.12). This is represented by a narrow band of negative feedback in Figure 4.10b, towards the rightmost edge of the figure. This contribution is masked by the much stronger positive

feedbacks in the outer bands of clouds, and thus averages up as a positive term over the domain in Figure 4.8. Wing and Emanuel (2014) saw a similar effect in their non-rotating simulations, where deep clouds blocked incoming solar radiation at the moistest regions leading to a drop in shortwave heating, but not as strong as in our simulation hence only acting as a neutral term in the budget.

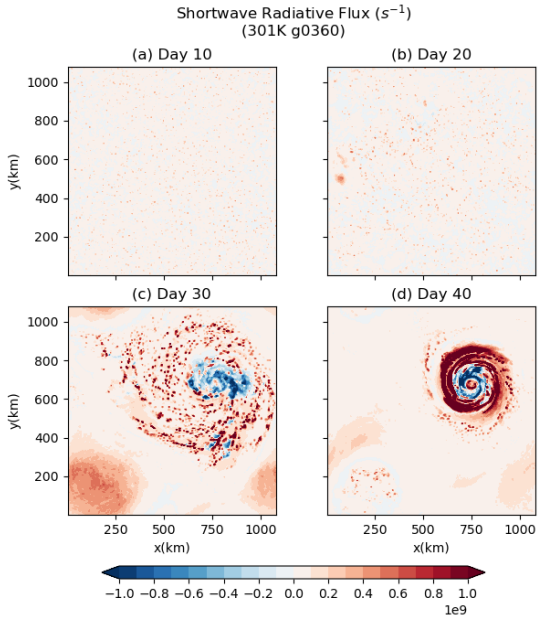

Figure 4.12 – Horizontal distribution of shortwave radiative feedback term on day 10, 20, 30 and 40 of simulation at 301K in 1080km domain.

Overall, the contribution from the shortwave radiative feedback term towards the FMSE variance budget is small, consistent to previous studies using rotating RCE simulations (Wing et al. 2016; Muller and Romps 2018; Carstens and Wing 2020). The distribution of shortwave feedback across the domain also resembles that of non-rotating self-aggregation experiments (Wing and Emanuel 2014; Holloway and Woolnough 2016).

Longwave Feedback

The strength of longwave feedback at the initial stages of our simulations are notably weaker than in earlier rotating RCE studies compared to other feedback terms. Longwave feedbacks were found to contribute equally as surface fluxes to the initial development (Wing et al. 2016; Muller and Romps 2018). Despite the enhancement of longwave feedback before genesis, its magnitude is still considerably lower than in the literature, far from being the leading order controlling factor to cyclogenesis. However, the distribution of the longwave feedback in Figure 4.10a mostly resembles non-rotating RCE simulations, especially Wing and Emanuel (2014).

Here we focus on the 5 days leading to genesis where the longwave term experiences the largest change. Although in Figure 4.10a, the change in magnitude of the longwave term during this period is masked by the normalization by $\{\widehat{h}'\}$, it is evident that during the early stages of aggregation the positive contribution comes from both the driest and moistest regions prior to the formation of the cyclone. The contribution from the dry region was also seen by Wing and Emanuel (2014), but not by Holloway and Woolnough (2016). In the driest area, Figure 4.11a shows the drying up of the mid to upper troposphere, which leads to reduced longwave cooling due to decreased emissivity. This is slightly opposed by the longwave cooling at the lower, moist atmosphere. Overall, this gives a positive feedback before genesis.

However, the longwave feedback transitions from strongly positive to weakly negative in the dry region after genesis, accompanied by decreasing moisture contents in the lower troposphere. A similar trend was observed by Wing and Emanuel (2014), after the non-rotating cluster is established. Using a simple two-layer model, they suggested that column longwave cooling is subject to the variations in emissivity at different levels. They argued that with amplifying dryness in the lower troposphere, a decrease in emissivity would lead to reduced longwave cooling, causing a positive longwave feedback at the dry region. This is one plausible explanation for what we see in our simulations, but we are not able to verify whether this is a clear-sky effect as in Wing and Emanuel (2014), due to the lack of clear-sky and cloud-only radiative flux outputs from our model.

Regarding the moistest region, it is a strong positive feedback throughout the simulation, consistent with most studies. It is commonly agreed among literature that it is a cloud effect, where deep clouds in the moist, high $\widehat{h}'$ regions reduce longwave cooling by its high opacity and low cloud top temperatures (Wing and Emanuel 2014; Wing et al. 2016). Overall, the patterns longwave radiative feedback in our simulation largely resembles the results from non-rotating simulations. However, the weaker magnitude of the radiative terms relative to other feedback terms (mainly the surface enthalpy flux) compared to other rotating RCE studies remains unexplained.

Surface Enthalpy Flux Feedback

In our simulations, the strong surface flux feedback throughout the simulation is in agreement with the majority of studies, being one of the dominant drivers of both self-aggregation and TC genesis simulations (Wing et al. 2016; Muller and Romps 2018; Carstens and Wing 2022).

At early stage, the surface flux feedback is positive at both the dry and moist patches. Decomposing the surface flux term into WISHE and air-sea disequilibrium feedback components following equation (9), it reveals that the strong positive feedback mainly comes from the WISHE effect (Figure 4.10d, e). The opposing air-sea disequilibrium effect is relatively weak prior to genesis. The combination of the two components creates a strongly net positive domain-mean surface flux feedback. This result is consistent with both rotating and non-rotating RCE studies, indicating that the WISHE is the dominant process in both self-aggregation and the subsequent spin-up of TC (Muller and Held 2012; Wing and Emanuel 2014; Wing and Cronin 2016; Wing et al. 2016; Muller and Romps 2018).

Following cyclogenesis, the surface flux feedback further amplifies with the sharp increase in wind speed near the TC center, as seen in Figure 4.3. It is accompanied by a rapidly strengthening WISHE feedback especially at the moist, high-$\hat{h}'$ region, indicating the increase in latent heat flux due to wind-enhanced evaporation. This is counteracted by a significant air-sea disequilibrium, due to the smaller near-surface mixing ratio difference. On the other hand, the much weaker winds at the dry regions compared to the cyclone core also creates a positive WISHE feedback, but not as strong as that in the moist vortex core. A negative air-sea equilibrium also existed in this region. Overall, the WISHE feedback overwhelms the air-sea disequilibrium effects in both moist and dry regions, like in Wing et al. (2016) and Muller and Romps (2018). Unlike non-rotating RCE where surface fluxes become a near-neutral or negative feedback due to disequilibrium effects (Wing and Emanuel 2014; Wing and Cronin 2016), strong winds associated with the development of a mature TC generates a positive feedback, leading to further intensification of the cyclone. This agrees with our current understanding on mechanisms sustaining TC development, where the main source of energy is latent heat flux through strong evaporation (Zhang and Emanuel 2016; Murthy and Boos 2018).

To summarize, surface enthalpy flux feedback is the dominant process leading to TC genesis, both at the early and mature stages of the simulation. The WISHE effect due to strong cyclonic

winds near the TC supplies large amount of sensible and latent energy, matching with traditional TC theories. Relative to the surface fluxes, the radiative terms are smaller than in literature. While the shortwave radiative fluxes are consistently weakly positive, the positive longwave radiative feedback mainly comes from the moistest regions throughout the simulation, owing to the reduction of radiative cooling by the greenhouse effect of deep convective clouds.

5 Sensitivity Experiments

In this section, various sensitivity tests are carried out to investigate the dependence of TC genesis in our simulations to environmental parameters, including SST, domain size and the presence of mean wind, as described in section 3.1.2.

5.1 Sea Surface Temperature (SST)

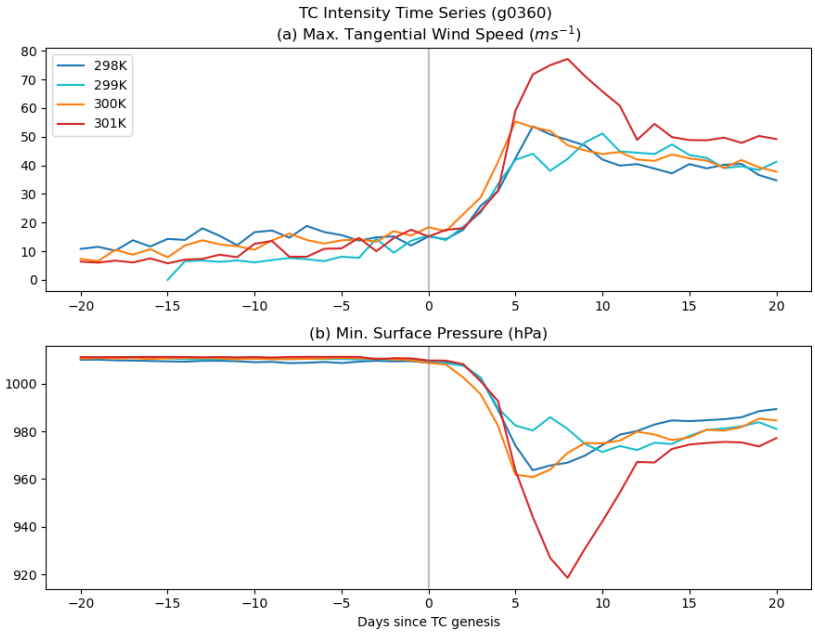

Figure 5.1 - Time series of (a) maximum tangential wind speed (ms^{-1}), (b) minimum surface pressure (hPa) of simulations at 298-301K SSTs in 1080km domain, aligned to the TC genesis time.

Three additional simulations are run with the exact same model setups as in section 4, except the SST is varied between 298K and 300K at 1K intervals as discussed in 3.1.2. Figure 5.1 shows the evolutions of maximum tangential wind speed and minimum surface level pressure in the four runs, which represent the intensity of the TCs over time. Due to large variations in genesis time across different runs, the time series are aligned to the time of genesis. It could be seen that the TCs intensify at similar rates in the first 5 days following genesis. Out of the 4 SSTs, the cyclone at 301K deepens the most, accompanied by the strongest tangential winds. A strong decline is observed after the TC reaches maximum intensity. The other 3 SSTs generated cyclones of similar strengths, which then roughly sustain their intensities and gradually weaken over time. The warmest run reaches an intensity of roughly 30% stronger in terms of maximum tangential wind speed. When the cyclones stabilize roughly 15 days after genesis, the warmest SST showed the strongest intensity while the coolest is the weakest, both in terms of wind speed and pressure. However, the SST dependence remains unclear as the

simulations with intermediate SSTs do not show a clear upward trend of TC intensity with warming. This contradicted with theoretical predictions of more intense cyclones with warming oceans (Chavas 2013; Khairoutdinov and Emanuel 2013; Ramsay et al. 2020). However, caution is required in interpreting our results as a large degree of stochasticity in the model exists, depending on the initial soundings (Wing et al. 2016). A possible future direction would be running an ensemble of simulations for each SST, while adopting a wider range of SSTs to observe the true variability of TC intensities.

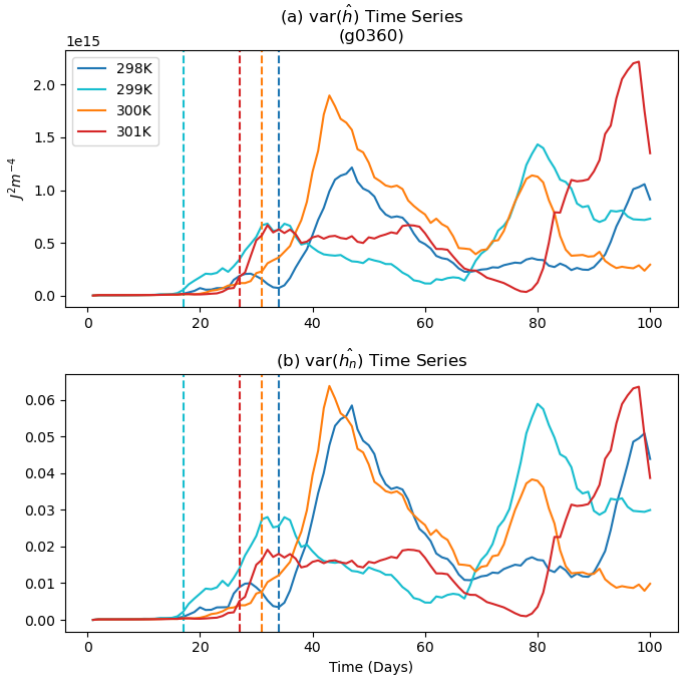

Figure 5.2 – Day 1-100 time series of (a) FMSE variance $var(\hat{h})$, (b) normalized FMSE variance $var(\hat{h}_n)$ of simulations at 298-301K SST in 1080km domain. Dotted lines represent genesis time of each SST run.

Similar to section 4, TC genesis at different SSTs is analyzed using the FMSE variance framework. In analogy to Figure 4.7, the evolution of FMSE variance in different SST runs are shown in Figure 5.2a. The timing and the magnitude of $var(\hat{h})$ varies greatly across SSTs. While cyclogenesis occur around 30 days in 298K, 300K and 301K runs, 299K is an outlier which took less than 20 days. 298K and 300K runs showed similar trends where a sharp peak in $var(\hat{h})$ forms corresponding to the first cyclone, which then gradually decayed and forms another smaller peak as the upper-level cyclone emerges and replaces the TC. On the other hand, 299K and 301K runs sustains at a weaker aggregated state for the first cyclone, which then develops into higher $var(\hat{h})$ values at the later stage. Although the cyclone in the 301K run is distinctively strong (Figure 5.1), no signs of stronger aggregation is observed in terms of $var(\hat{h})$.

Visually, the maxima of each time series increases with SST, albeit occurring at different timings, owing to a theoretically higher capacity of water vapor in warmer atmospheric profiles. To allow a fair comparison between variance budgets of across SSTs while using the FMSE variance framework, the variances and its budget terms are normalized as described in section 3.2.3, adopting the approach taken by Pope et al. (2021). Following normalization, aggregation measured by $var(\hat{h}_n)$ reaches a similar level as depicted in Figure 5.2b, consistent to the non-rotating RCE simulations by Pope et al. (2021).

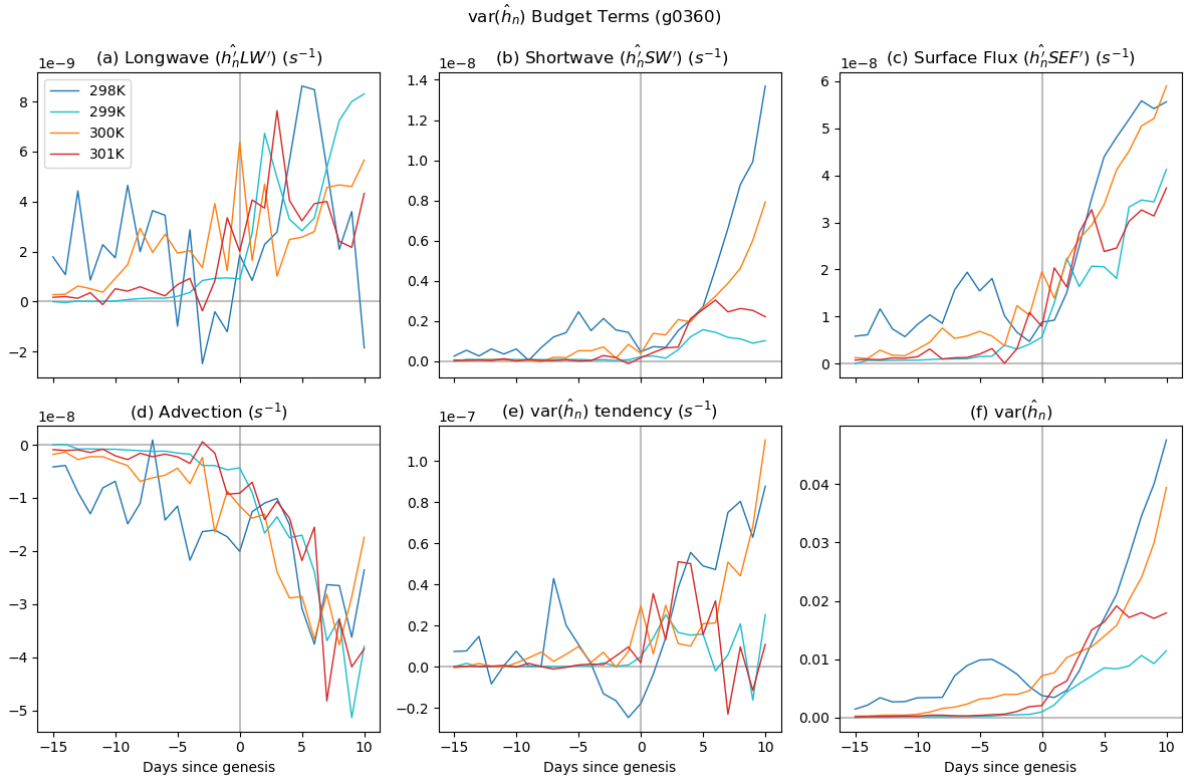

Figure 5.3 –Time series of (a) Longwave radiative flux, (b) shortwave radiative flux, (c) surface enthalpy flux, (d) advective term. (e) and (f) are the tendencies and values of $var(\hat{h}_n)$. All time series are aligned to the time of TC genesis. Values taken from simulations at 298-301K SST in 1080km domain. Note that the scale of y-axis differs across plots.

In order to compare the contributions from various radiative-convective feedback processes at different SSTs, the evolution of FMSE variance, its tendency and all budget terms are shown in Figure 5.3, aligned to the time of TC genesis. Note that all feedback terms are normalized by $\hat{h}_{max} - \hat{h}_{min}$ in the figures. In Figure 5.3f, the evolution of $var(\hat{h}_n)$ are similar across SSTs: $var(\hat{h}_n)$ slowly increases 5 to 10 days prior to genesis, followed by a sharp rise after genesis. The only exception is 298K, where a peak in $var(\hat{h}_n)$ forms before genesis. Upon inspection on PW and OLR plots, the moist patch first forms a coherent cluster, which then re-organizes and forms a vortex afterwards. This process is not observed in the other 3 simulations,

which show similar $var(\hat{h}_n)$ tendencies before genesis. Following genesis, the trends of $var(\hat{h}_n)$ tendencies split into two groups, as previously discussed. With different aggregation pathways taken by various runs, there is no evidence of the dependence of aggregation rate on SST, contrasting Pope et al. (2021) who observed an increase in rate of change of aggregation with SST.

Decomposing the variance budget into individual feedback terms, the surface enthalpy flux term is consistently the largest term across all SSTs (Figure 5.3c). It is a positive feedback throughout the simulations, with its magnitude significantly increases as the TCs intensify rapidly after genesis, together with the increase in surface wind speed. The time series of surface enthalpy fluxes are visually similar to $var(\hat{h}_n)$, suggesting that it is the dominant term contributing to cyclogenesis and subsequent maintenance of the TC. No obvious trend is observed between SST and the magnitude of surface flux, apart from features due to different development pathways taken by each run such as the peak before genesis at 298K, and the division into two groups of stronger and weaker fluxes.

Similar trends are observed for the shortwave radiative feedback term. The shortwave term is steadily weakly positive at the early stages, consistent with previous non-rotating and rotating RCE studies. It then increased greatly with $var(\hat{h}_n)$ following genesis, due to the strong tie between FMSE and shortwave heating rates as previously discussed. Meanwhile, the evolution of longwave feedback is relatively noisy and varies greatly across SSTs. Finally, the advection term is always negative, exporting FMSE from moist to dry regions, reducing spatial moisture variability. It is increasingly negative as the TC intensifies.

Due to disparities in TC development among different runs, the sensitivity of FMSE variance and feedback terms are difficult to be analyzed by aligning the genesis timings. In view of this, Figure 5.4 displays the relationship between each term and $var(\hat{h}_n)$, following the approach by Pope et al. (2021) and Carstens and Wing (2022). By averaging each feedback term within 20 evenly spaced $var(\hat{h}_n)$ bins between 0 and 0.08, the strength of each term at different stages of cyclogenesis, quantified by the degree of self-aggregation, could be analyzed and compared to other SST runs.

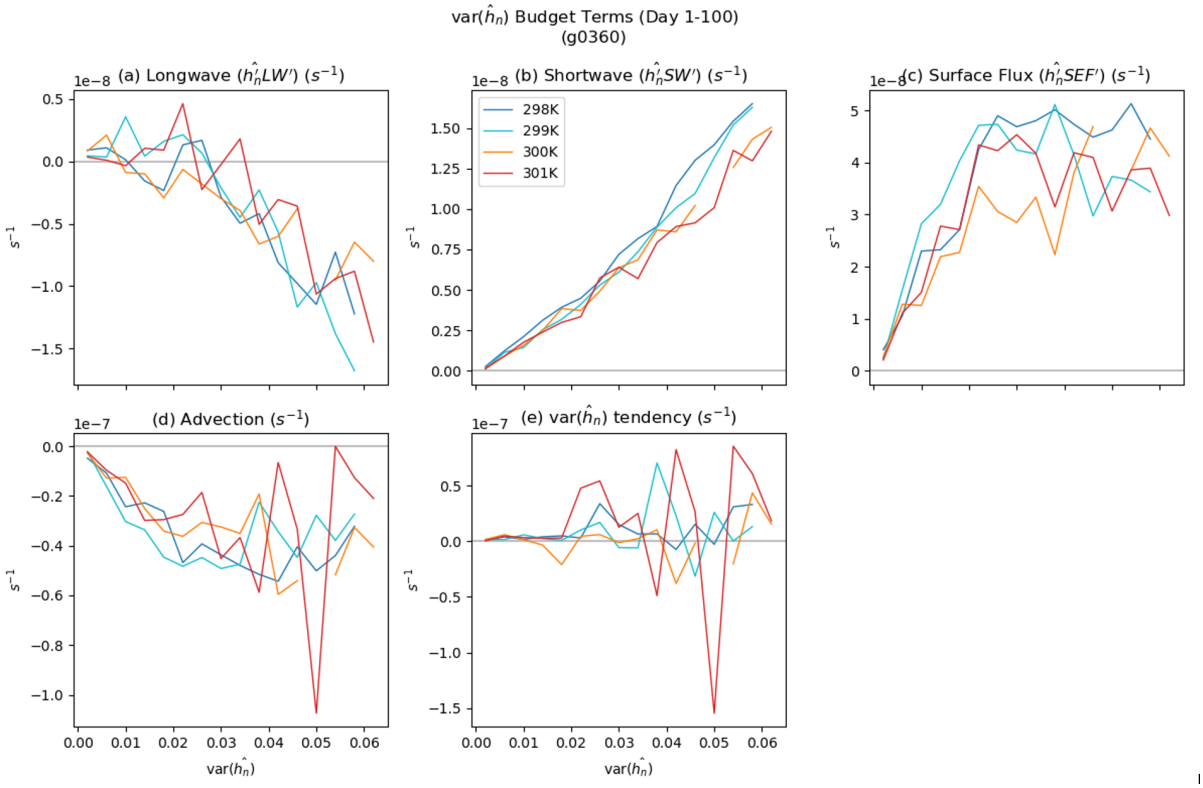

Figure 5.4 – Mean of each FMSE variance term against normalized FMSE variance, calculated for 20 evenly spaced $var(\hat{h}_n)$ bins. (a) Longwave radiative flux, (b) shortwave radiative flux, (c) surface enthalpy flux, (d) advective term. (e) is the tendencies of $var(\hat{h}_n)$. Breaks exist due to the absence of data points within the corresponding bin. Data taken from Day 0-100 of simulations at 298-301K SST in 1080km domain.

From Figure 5.2b, $var(\hat{h}_n) < 0.02$ roughly corresponded to the growth phase of the convective cluster, where $var(\hat{h}_n)$ tendency is mostly positive (Figure 5.4e). However, some noise existed since data from day 0 to 100 are used in creating these plots. As previously mentioned, the cyclones do not sustain their strength upon maturity and interact with an upper level cyclone, which cause dissipation and the formation of a new cyclone, while the variances and budget terms greatly fluctuate (Figure 5.2). With this regard, only the first 50 days of simulations are considered in the previous discussion. However, insufficient data points are available to create Figure 5.4, therefore the full 100-day time series are used. Caution is required in interpreting these figures as values from the weakening phase of TC could possibly interfere with the results.

Considering the longwave term, it could be seen that Figure 5.4a is much less noisier than Figure 5.3a. At the initial stages of self-aggregation, the longwave feedback is weakly positive, followed by a clear downward trend in longwave feedback as $var(\hat{h}_n)$ increased, which causes

it to become a negative term at the mature stage. However, the sensitivity of the longwave feedback term to SST is relatively unclear.

A clear positive relationship exists between the normalized shortwave term and $var(\hat{h}_n)$, while the strength of feedback also decreases with warmer SSTs. Both results resembles findings by Pope et al. (2021). The former is due to the enhanced absorption of shortwave radiation by water vapor at moist regions with increased aggregation. Concerning the sensitivity to SST, Pope et al. (2021) argued that column water vapor increases exponentially with SST, but shortwave heating increases logarithmically with water vapor, causing a near-linear increase in shortwave heating rates with SST. Meanwhile, the theoretical limits of FMSE are largely controlled by the water vapor content, hence increases exponentially with SST. Therefore, upon normalization by $\hat{h}_{max} - \hat{h}_{min}$, the shortwave feedback term decreases with SST (Pope et al. 2021).

The surface enthalpy flux terms show similar trends across the runs, without strong signs of dependence on SST. At initial stages of aggregation ($var(\hat{h}_n) < 0.02$), the surface fluxes increase rapidly due to the increase in surface wind speed, which then plateau when $var(\hat{h}_n)$ further increase. The converse is true for the advective term, where it becomes more negative but maintained a similar value upon maturity. This contrasts with Pope et al. (2021) as they found a less negative contribution from the advection term with warmer SSTs.

To conclude, the sensitivity of TC genesis and intensity remains unresolved. The dependence of feedback processes on SST in spontaneous tropical cyclogenesis in our simulations is also unclear. In the future, a larger range of SSTs and ensembles of simulations could be employed to clarify our findings, while the use of FMSE variance budget in analyzing TC genesis still awaits further exploration.

5.2 Domain Size

The motivation of this sensitivity test is primarily due to the formation of an upper-level cyclone at the 'antipode' point of the surface TC, which then interacts and competes with the latter for moisture, eventually replacing the surface cyclone (detailed discussed in section 4.1). This phenomenon was rarely reported in relevant literature, and might be purely artificial due to the convergence of TC outflow in the biperiodic domain. Since this process involves major reorganization of water vapor and clouds within the domain, it interferes with our analysis involving FMSE variance and relevant feedback processes. Therefore, it is of interest to test if such phenomenon is sensitive to the domain geometry of the previous simulations. The impact of the second cyclone to the FMSE budget and feedback processes could be minimized if its formation is suppressed in our new simulations.

Figure 5.5 shows the snapshots of column PW of the simulation with a square domain of side 2304 km, at the same SST of 301K as in the control run. Qualitatively, the domain is moister, roughly 1 cm higher in the PW field than in 1080 km simulation, due to a different sounding adopted. In the 1080 km runs, the initial soundings are taken from the mean of the final 30 days in a smaller domain RCE as described in 3.1.1. However, these soundings are drier than usual, possibly due to the absence of a minimum wind speed seen by the surface flux scheme, leading to reduced moisture. Instead, a moist neutral sounding from Rotunno and Emanuel (1987) is adopted to solve this issue, therefore causing the moister background in comparison.

Initially, the convective cells follow a similar pathway of self-aggregating into larger clusters, while dry patches expand at the same time. By day 25, multiple moist patches form instead of one coherent cluster, which correspond to regions of positive vorticities in Figure 5.6. These moist vortices then combine into a single dominant vortex by day 30. This development pattern resembles the 'vortex merger' process described by Davis (2015). However, they observed 'vortex merger' at a much smaller domain (960 km), while our 1080 km runs did not demonstrate such process. Reaching maturity, the TC has a radius of roughly 400km, doubling the size of the control run (Figure 4.2f). It is hypothesized that due to the enlargement of the domain (4 times the original size), more room is available for the subsidence of air outflow from the top of the TC. There is also a higher abundance of moisture across the larger domain, both supporting the formation of a larger cyclone.

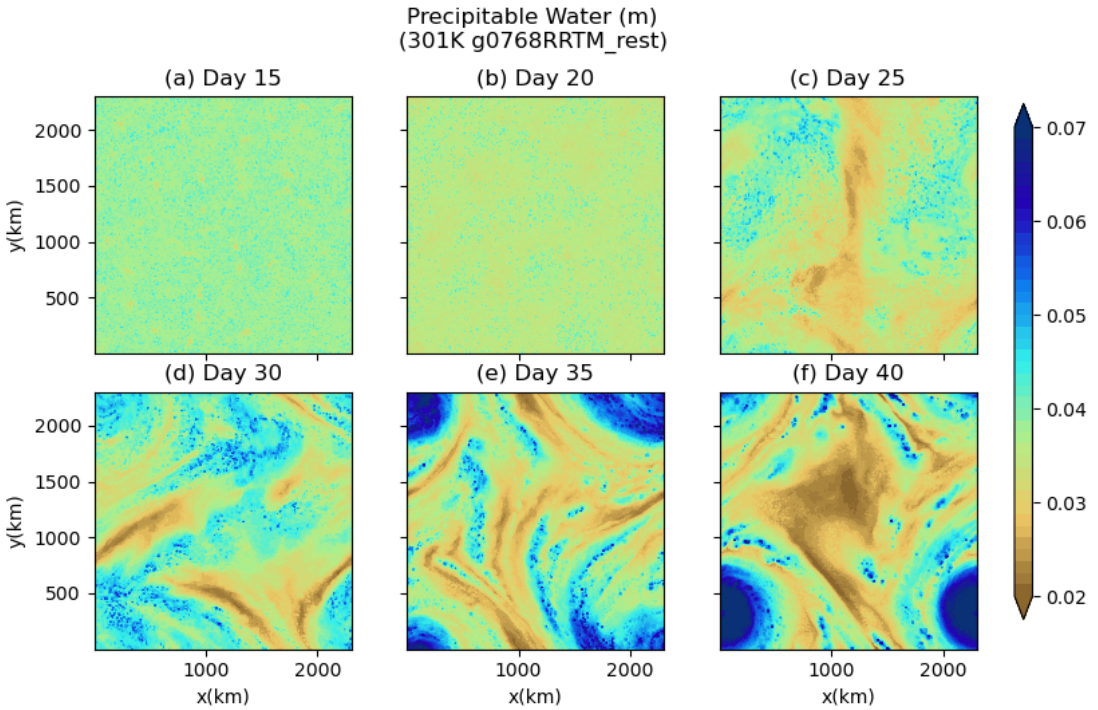

Figure 5.5 - Instantaneous snapshots of precipitable water (m) on days (a) 15, (b) 20, (c) 25, (d) 30, (e) 35 and (f) 40 for simulation at 301K in 2304 km domain.

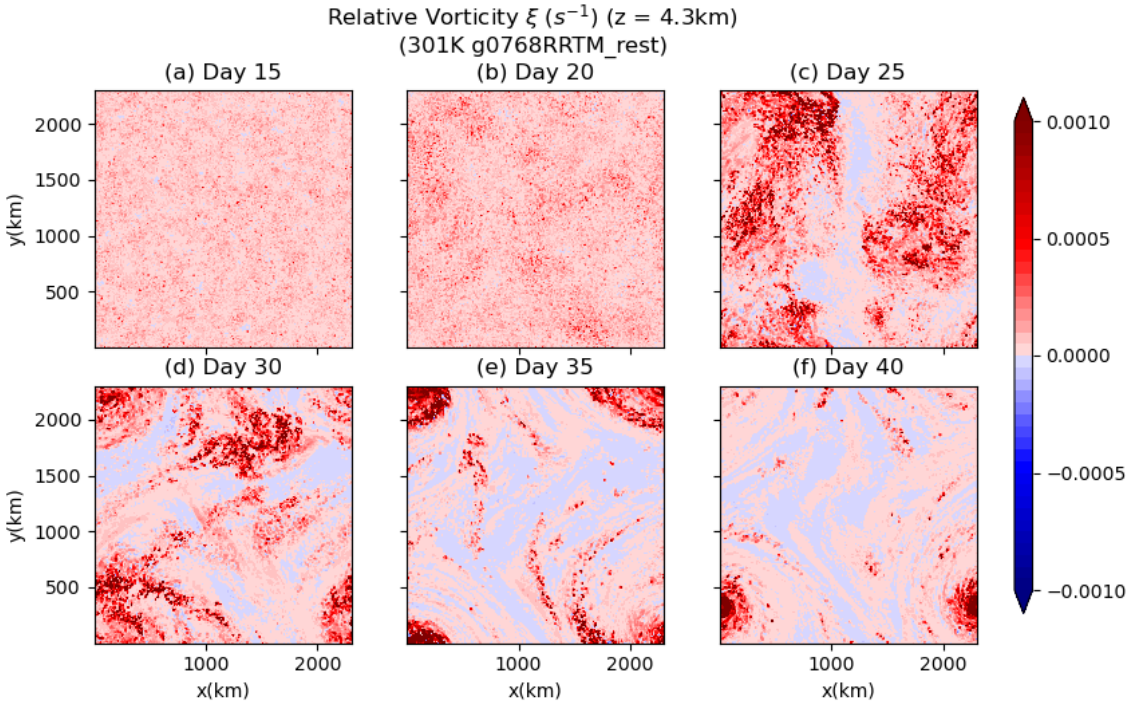

Figure 5.6 - Instantaneous snapshots of relative vorticity at 4.3km height (s^{-1}) on days (a) 15, (b) 20, (c) 25, (d) 30, (e) 35 and (f) 40 of simulation at 301K in 2304 km domain.

Reaching maturity of the TC, an upper-level cyclone is not observed at the opposite side of the domain. Although areas of positive vorticity with semi-coherent cyclonic structures are present at heights above 7 km (not shown), the vortex do not extend towards lower levels with time. Limited interactions are present between the TC and the upper cyclone, where dissipation is not observed at least during the first 63 days. Although a full 100-day simulation is not done due to constraints on time and computing resources, it is still valuable to compare results from the large domain to the control run, in order to test the robustness of the results with or without the influence of the upper-level cyclone.

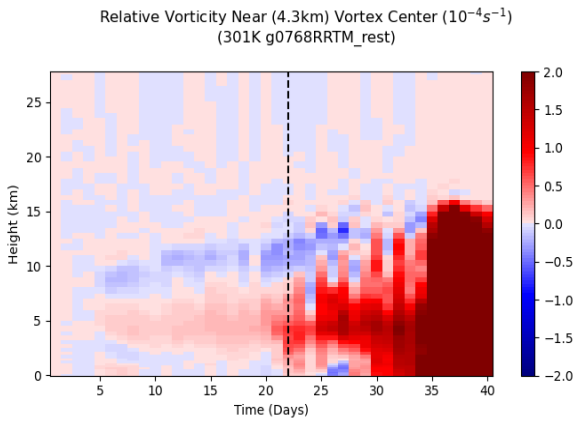

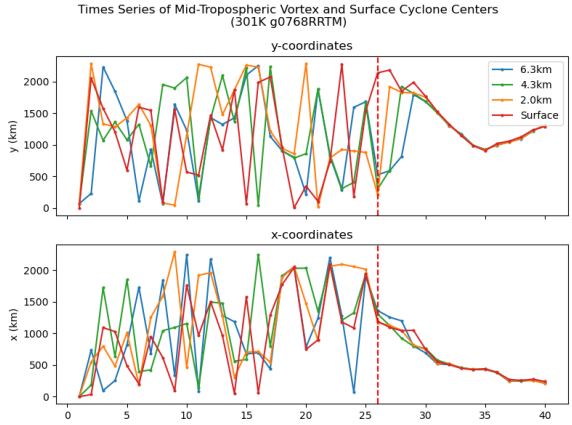

(Left) Figure 5.7 - Hovmöller diagram of daily column relative vorticity (s^{-1}), averaged in a 150 x 150 km box around the 4.3 km height vortex center. Vortex center is tracked by the point of daily maximum relative vorticity smoothed over a 150 x 150 km box. Data taken from simulation at 301K in 2304 km domain.

(Right) Figure 5.8 - Time series of vortex center coordinates at surface, 2.0 km, 4.3 km, and 6.3 km heights. All vortex centers follow the same definition in Figure 5.7, except for the surface which is defined as the point of minimum surface pressure. Vertical dotted lines represent the genesis time. Data taken from simulation at 301K in 2304 km domain.

Upon inspection on relative vorticity profiles following the mid-level vortex, the emergence of the surface cyclone is again, preceded by a mid-level vortex at 4 – 6km (Figure 5.7). However, the trajectories of the vortex centers varied greatly (Figure 5.8), in addition to the mismatch between upper and lower levels vorticity centers, due to the presence of multiple vortices prior TC genesis, consistent to Davis (2015).

The evolution of FMSE variance and the budget terms are shown in Figure 5.9 and 5.10. The evolution of $var(\hat{h})$ is similar to Figure 4.7, where the variance increased quickly following TC genesis. However, the rate of change is lower compared to the smaller domain run, taking roughly double the duration to reach maximum degree of aggregation. The slower

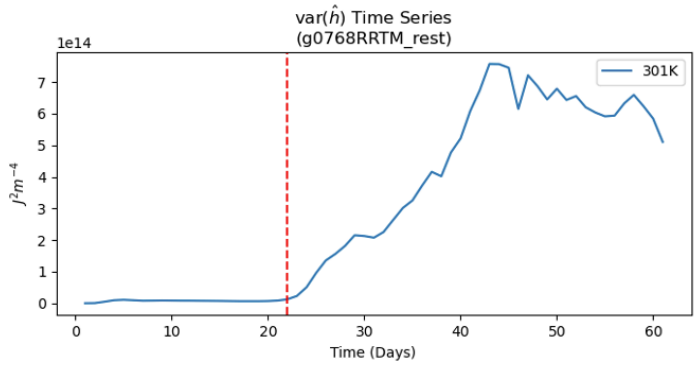

Figure 5.9 - Day 1-50 time series of FMSE variance of simulation at 301K in 2304km domain. Vertical dotted line represents the genesis time.

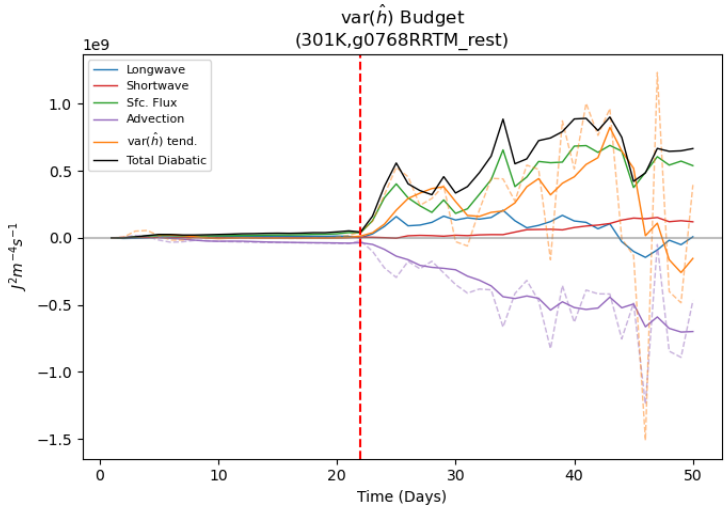

Figure 5.10 - Day 1–50 Time series of domain-mean FMSE variance budget terms of simulation at 301K in 2304 km domain. Diabatic terms (longwave flux, shortwave flux, and surface enthalpy flux) are derived and plotted from daily instantaneous model outputs. Solid lines for advection term and $var(\hat{h})$ terms are 5-day running averaged, while dotted lines show the daily instantaneous values. Vertical dotted line represents the genesis time.

development resembles the 298K and 300K simulations in Figure 5.2. Otherwise, $var(\hat{h})$ is relatively stable compared to the control run. This is an encouraging finding, as the enlargement of the domain might have prevented undue interference in the evolution due to the upper-level cyclone.

The FMSE variance tendency is further decomposed into individual budget terms in Figure 5.10. At the early stage, the surface flux term, in relative to other feedback terms, is smaller than in the control run. Further partitioning reveals that the WISHE feedback is weaker in the large domain run (Figure 7.3), while the air-sea disequilibrium effect remains insignificant. The remaining feedback terms behave largely identical to the control simulation.

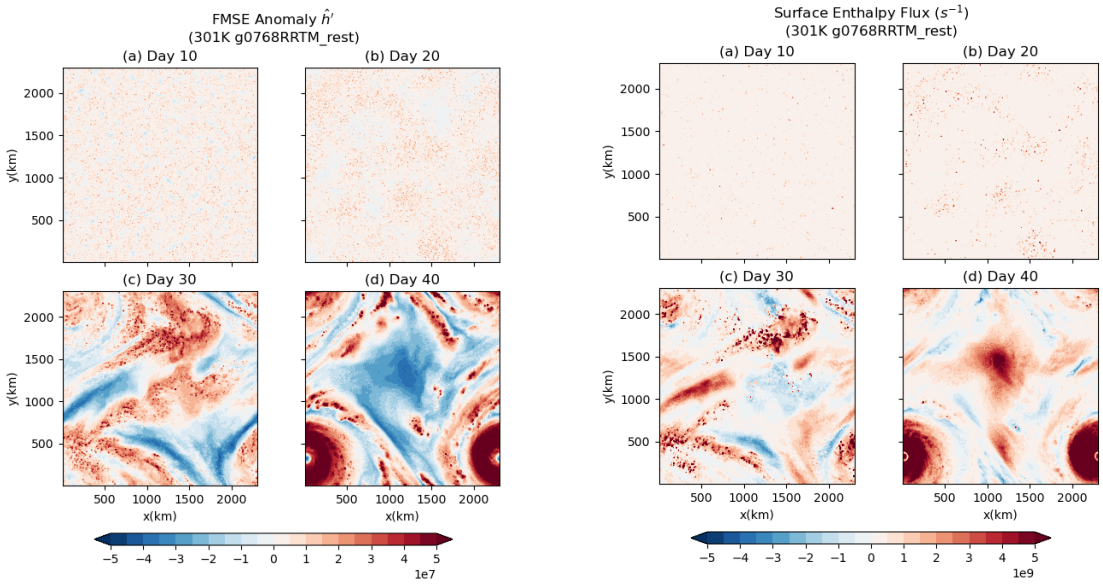

Figure 5.11 - Snapshots of vertically integrated FMSE anomalies on day (a) 10, (b) 20, (c) 30 and (d) 40 of simulation at 301K in 2304km domain

Figure 5.12 - Snapshots of surface enthalpy flux term on day (a) 10, (b) 20, (c) 30 and (d) 40 of simulation at 301K in 2304km domain

Following genesis, the surface flux feedback exhibits differential behavior compared to the control run. Instead of rapidly increasing shortly after genesis, the surface flux term gradually increases over 10 – 12 days, where its magnitude is roughly comparable to the longwave radiative feedback in the first 5 days. Plots of spatial distribution of FMSE anomaly ($\hat{h}'$) and the surface flux term suggest that this is due to the absence of the upper-level cyclone at the dry region. Figure 4.9c shows that the upper-level cyclone corresponds to a coherent vortex of strongly negative $\hat{h}'$ on day 30, due to the extreme dryness in the area initially. It then gradually transitioned into a circular patch of weakly positive $\hat{h}'$, following the moistening of the vortex. Due to the significantly low $\hat{h}'$ around the timing of TC genesis, its correlation with the surface flux anomaly ($\hat{h}'SEF'$) is strongly positive at the dry region when combined with the significantly below-average wind speed away from the surface cyclone (Figure 5.13c). This results in a strongly positive surface flux feedback averaged over the domain. However, such contribution from the dry patch is absent in the 2304 km domain. The $\hat{h}'$ at the outer regions of the surface cyclone is moderately negative (Figure 5.11c), which is not able to generate a strong surface flux feedback (Figure 5.12c). Around day 40, the positive surface flux feedback mainly comes from the surface cyclone in both simulations, therefore showing similar behavior in Figure 4.8 and 5.10. Since the advection term is calculated as the residual of $var(\hat{h})$ tendency, it is also correspondingly smaller in the large domain runs.

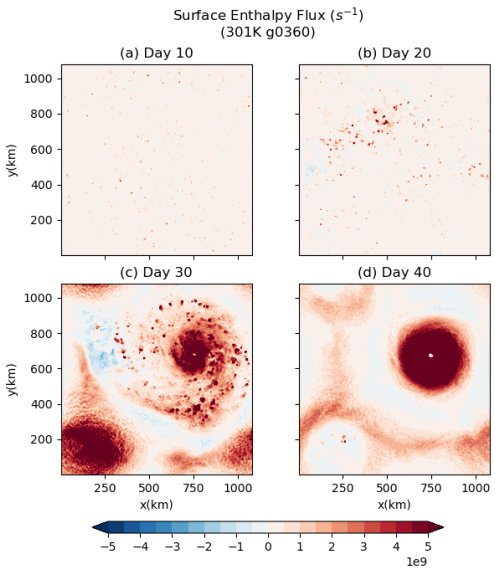

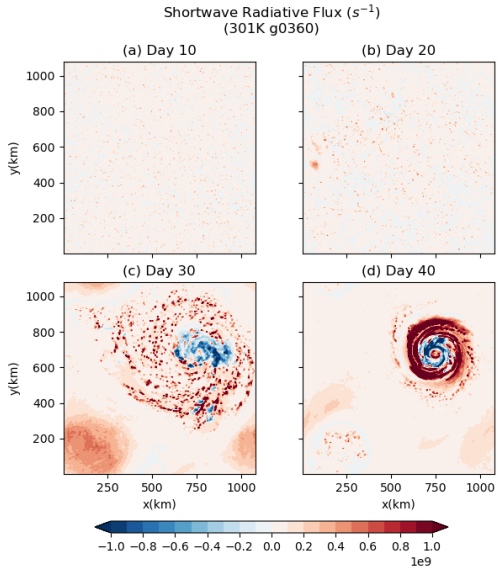

(Left) Figure 5.13 - Snapshots of surface enthalpy flux term on day (a) 10, (b) 20, (c) 30 and (d) 40 of simulation at 301K in 1080km domain

(Right) Figure 5.14 - Snapshots of shortwave radiative feedback on day (a) 10, (b) 20, (c) 30 and (d) 40 of simulation at 301K in 1080km domain

Another notable difference is the shortwave radiative feedback. At the mature stage, the shortwave feedback in the large domain run strengthens with time, which eventually overtakes longwave feedback as the second largest diabatic term in the variance budget (Figure 5.10). The increased importance of shortwave feedback arises from the dry region, where patches of moderately negative $\hat{h}'$ corresponds to strong positive shortwave feedback at day 40 (Figure 5.11d and 5.15d). Together with the strongly positive contribution from the cyclone core, this produces a fairly strong feedback in the mature stage of TC development. Contrastingly, the small domain run has a weaker shortwave feedback due to the weakly positive $\hat{h}'$ at the upper-level cyclone (Figure 5.14d).

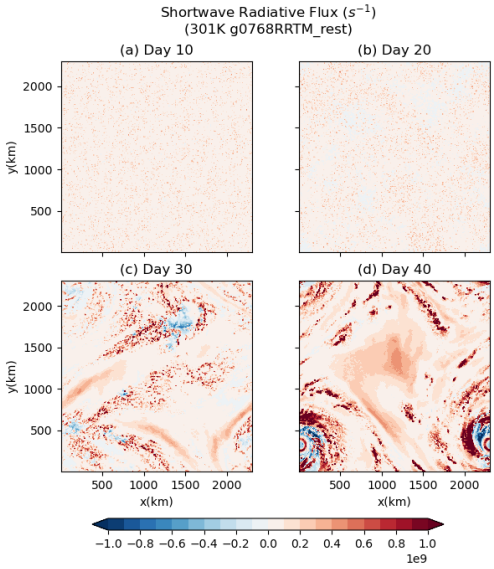

Figure 5.15 - Snapshots of shortwave radiative feedback on day (a) 10, (b) 20, (c) 30 and (d) 40 of simulation at 301K in 2304km domain

Overall, the FMSE variance budgets of the simulations are sensitive to the choice of domain size, particularly during the mature stage of the TCs. The evolution of FMSE variance is influenced by the reorganization of moisture and clouds due to the interaction between surface and upper-level cyclones. The strength of the surface enthalpy flux feedback and shortwave feedback are prone to be affected by the upper-level cyclone. Therefore, bias might exist for our analysis in section 4, but the results for the pre-genesis period are proven robust. A possible future direction would be carrying out the same set of simulations using a larger domain, in order to minimize the impact of artificial effects introduced by the domain geometry. Also, this raise concerns on the interpretation of results from various simulations done in the literature, due to the wide range of domain sizes adopted. More careful investigation is required to avoid potential impacts from features introduced artificially, such as the upper-level cyclone in this study.

5.3 Prescribed Mean Wind

In most cloud resolving RCE simulations, the horizontal resolution well captures large scale clouds and convective activities, but fails to resolve turbulence and eddies in the boundary layer (Naumann et al. 2017; Mol et al. 2019), causing a lack of convective gustiness in the models. Together with the absence of tropical large-scale circulations in idealized models, there might be a distinct lack of winds in the lower troposphere, causing a deficiency in surface fluxes particularly at the dry regions. Strong air-sea disequilibrium effects might place the dry atmosphere at a 'wind-limited regime', which is highly sensitive to any winds that might trigger strong evaporation. With this regard, parameterization of surface exchange processes in these models employs a minimum wind speed threshold to compensate for unresolved latent and sensible heat fluxes (e.g., Wing and Emanuel 2014; Mol et al. 2019). For example, System for Atmospheric Modelling (SAM) uses a threshold of 1 ms^{-1} where winds at calm areas are artificially raised to this value when calculating fluxes.

However due to technical difficulties in compiling the model, such threshold is not implemented to our simulations. Instead, we attempted to add a mean wind of $3ms^{-1}$ throughout the troposphere, in order to prevent instabilities that might arise due to the underestimation of winds, especially at dry regions. It is also anticipated that the instability might be one of the causes of the formation of the second cyclone. Therefore, the behavior of spontaneous TC genesis in the presence of a prescribed mean wind compared to a resting background wind is of interest.

Quantitatively, the evolution of variables such as relative vorticity and PW largely resembles the large domain resting simulation (Figure 5.16). The time taken for the TC to reach tropical storm intensity is 26 days, slightly later but probably due to the dependence on initial conditions. Again, no upper-level cyclone is observed apart from a small patch of positive vorticity at around 7 – 10 km, which do not strengthen nor extend towards the surface. Despite the introduction of a mean wind would possibly cause vertical wind shear, TC genesis is not prevented under its influence.

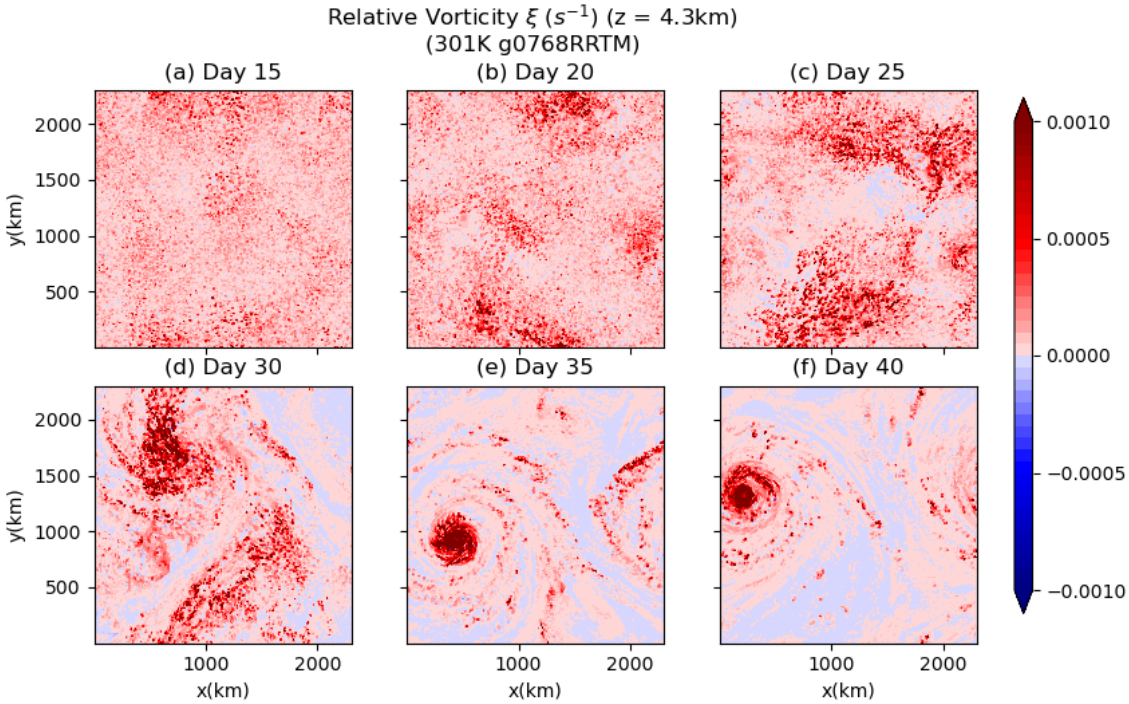

Figure 5.16 – Instantaneous snapshots of relative vorticity at 4.3km height (s^{-1}) on days (a) 15, (b) 20, (c) 25, (d) 30, (e) 35 and (f) 40 for simulation at 301K in 2304 km domain with 3ms^{-1} prescribed mean wind.

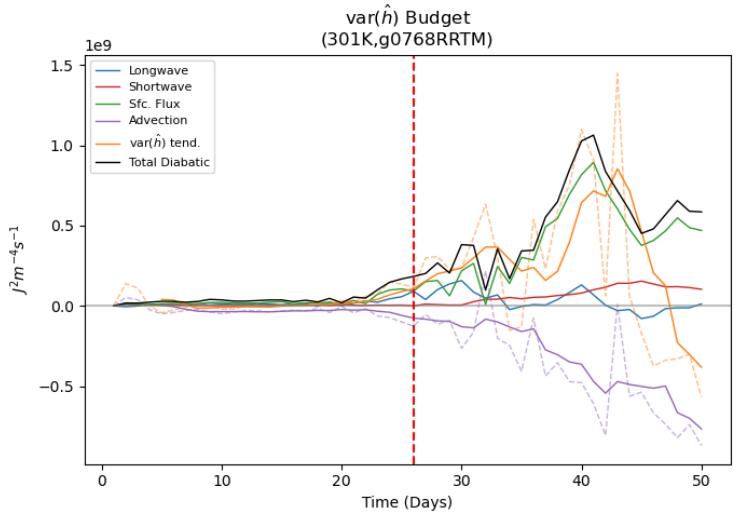

Figure 5.17 - Day 1–50 Time series of domain-mean FMSE variance budget terms of simulation at 301K in 2304 km domain with 3ms^{-1} prescribed mean wind. Diabatic terms (longwave flux, shortwave flux, and surface enthalpy flux) are derived and plotted from daily instantaneous model outputs. Solid lines for advection term and $var(\hat{h})$ terms are 5-day running averaged, while dotted lines show the daily instantaneous values. Vertical dotted line represents the genesis time.

Considering the FMSE variance budget, more fluctuations are observed within all feedback terms during the early stages, while being much steadier in the resting simulations (Figure 5.10). The relative contributions from each feedback following TC genesis are also mostly consistent. In particular, the surface flux feedback slowly increases after genesis similar to the resting run, but reaches a higher peak in variance at day 40. Contrastingly, Carstens and Wing (2022) suggested that the implementation of a higher wind speed when calculating surface fluxes might damp the surface flux feedback, due to smaller differences in fluxes between the windy and calm regions. Since the feedback term is calculated from the anomaly of domain-averaged surface flux feedback, a higher surface flux on average would decrease the magnitude of the positive anomalies hence lowering the domain-averaged feedback. It is hypothesized that our observations from the model might be purely stochastic, which causes the discrepancy.

This experiment gives results that are highly consistent with the resting simulation in the larger domain, except a stronger surface flux feedback term which contradicts the literature. More effort would be required in testing its robustness, such as running ensembles of simulations both with and without mean winds. Since an upper-level cyclone is absent in both large domain simulations while introducing mean wind does not cause significant impact, at least at early stages and shortly after TC genesis, the simulation without a mean wind would be a safer choice for interpretation, as the effect of increased wind speed and vertical shear on surface fluxes and is relatively uncertain.

6 Conclusions

This study adopts a rotating radiative-convective equilibrium (RCE) model to simulate spontaneous tropical cyclogenesis under idealized environments. Fixed sea surface temperatures (SSTs) around the threshold for tropical cyclogenesis are implemented. The formation of TC from homogeneous initial conditions is observed in all model runs, elapsing roughly 30 days on average. Early stage of the simulations largely resembles convective self-aggregation in non-rotating RCEs, where the formation of moist, convective clusters is accompanied by the enlargement of dry patches within the domain. A TC forms following the formation of a single, rotating deep convective cluster. Consistent to previous studies, a mid-tropospheric vortex forms preceding the spin-up of the surface cyclone in our simulations. With this regard, our simulations are coherent with TC genesis pathways in the real atmosphere, hence could be utilized to understand its underlying mechanisms.

Following the framework in studying convective self-aggregation in previous literature, a frozen moist static energy (FMSE) budget is implemented to quantify various feedback processes contributing to the generation of a TC given homogeneous initial conditions, with a focus on the period shortly before reaching tropical storm intensity. In the set of small domain simulations, FMSE variance increases with the enhanced aggregation and TC intensity. Considering various feedback process contributing to the FMSE variance budget, the surface enthalpy flux feedback is the leading order contribution towards both cyclogenesis and intensification, where the WISHE feedback dominated over the air-sea disequilibrium effect. The longwave radiative feedback is notably weaker than other rotating RCE studies in relative to other feedback terms, despite its spatial distribution mostly resembled self-aggregation in non-rotating studies. Shortwave radiative feedback is consistently small, agreeing with previous studies. However, an upper-level cyclone forms in our small domain simulations, which competed with and replaces the first cyclone at the later stages of simulation, possibly impacting our analysis that is reliant on the distribution of moisture thus FMSE variances.

Several experiments are carried out to test the sensitivities of TC genesis to SSTs, domain size and the presence of a prescribed mean wind. Cyclone intensities are similar across a small range of SSTs, except the warmest run which is 30% stronger than the rest in terms of wind speed, while no direct relationship between TC intensity and degree of aggregation is found. Following the normalization of FMSE variance budget against SSTs, various feedback

processes displayed similar evolutions in time. No strong signs of temperature dependence existed except the shortwave term, which decreased in the normalized budget with SST.

By increasing the domain size of our simulations, the formation of the upper-level cyclone is prevented. This has also lowered the surface flux feedback caused by the extremely dry upper-level vortex, increasing the relative importance of longwave radiative in the growth stage of the cyclone. This has caused the FMSE budget terms to be more consistent with the literature. Meanwhile, the addition of mean wind to the simulations does not induce a significant impact on top of domain enlargement. The expansion of the domain might be a more viable way in minimizing the influence by the interaction between the surface and upper cyclones, while avoiding uncertain impacts induced by the introduction of mean wind for simplicity.

In the future, more effort is required to test the robustness of the results in this paper. Due to the high sensitivity of the simulations to initial conditions, it is a challenge to discern between stochasticity and the variability induced by model environmental parameters. Some studies implemented an ensemble of simulations, in order to account for the randomness in assessing the true sensitivity. In addition, a larger range of SSTs is more desirable in assessing the dependence of cloud-radiative processes in TC genesis on warming, to avoid its effect being masked by the noise in the model.

Regarding improvements to rotating RCE simulations in studying tropical cyclogenesis in general, fixed SSTs are used for simulations where air-sea coupling effects are absent. Several studies have pointed out the importance of interactive surfaces on radiative processes and surface fluxes, which might be relevant to assessing their sensitivity to a warming climate. The use of FMSE variance framework might be a new direction for future efforts in analyzing the dependence of TC genesis on SSTs, as it is relatively novel and awaits further investigation.

7 Appendix

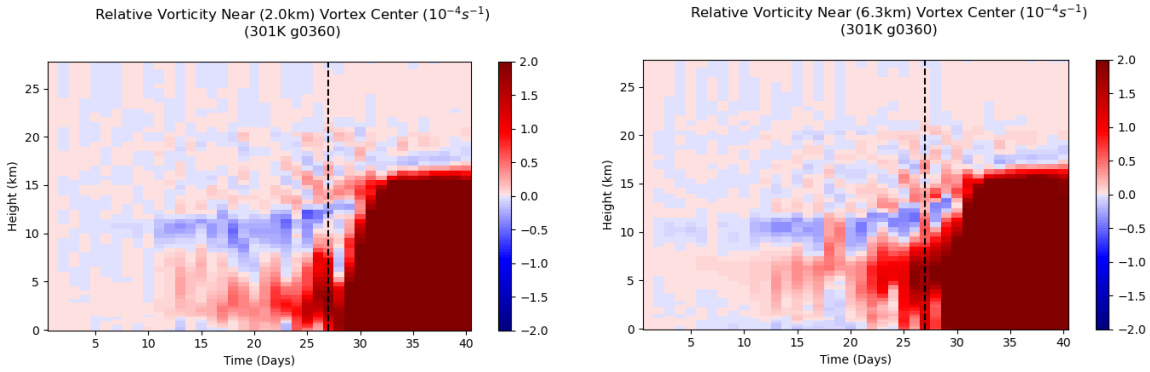

(Left) Figure 7.1 - Hovmöller diagram of daily column relative vorticity (s-1), averaged in a 150 x 150 km box around the 2.0 km height vortex center. Values taken from simulation at 301K in 1080 km domain.

(Right) Figure 7.2 - Hovmöller diagram of daily column relative vorticity (s-1), averaged in a 150 x 150 km box around the 6.3 km height vortex center. Values taken from simulation at 301K in 1080 km domain.

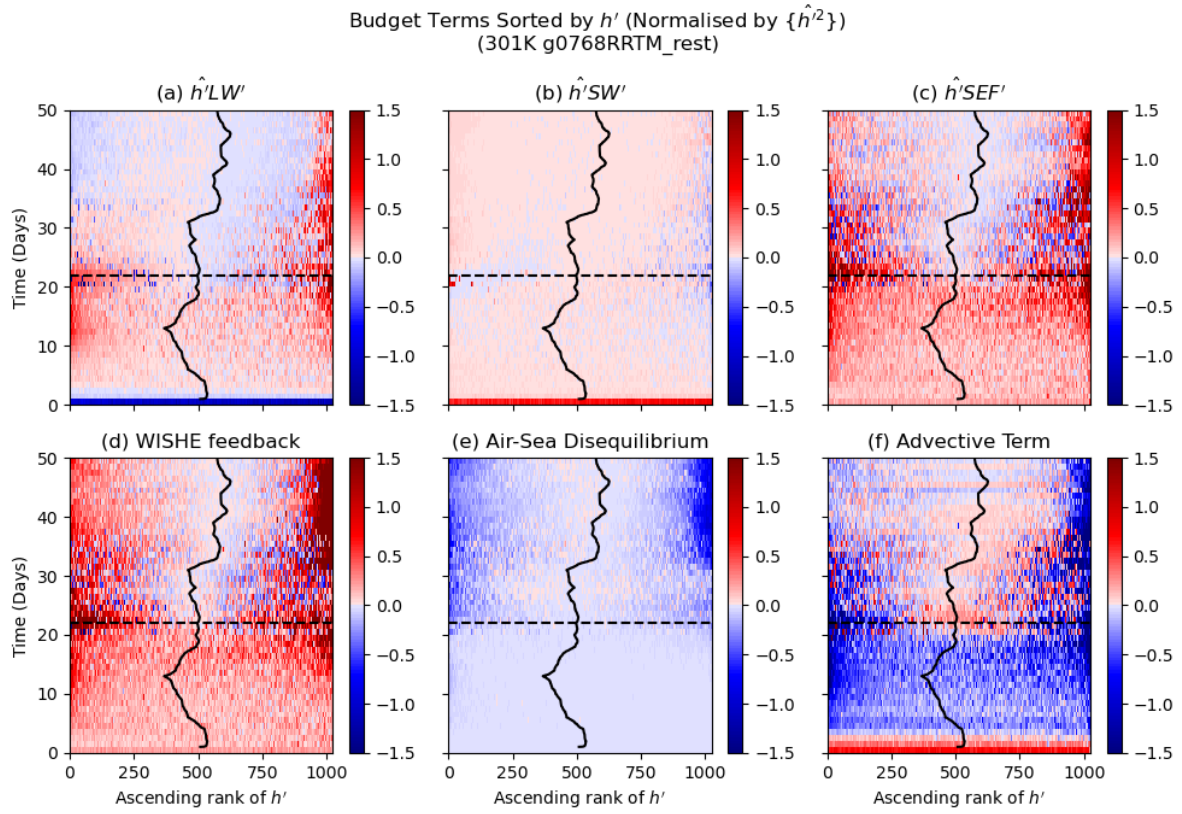

Figure 7.3 - Correlation between vertically integrated FMSE anomalies and anomalies of (a) longwave radiative flux, (b) shortwave radiative flux, (c) surface enthalpy flux, (d) surface enthalpy flux due to wind speed anomalies (WISHE feedback), (e) surface enthalpy flux due to air-sea disequilibrium anomalies, (f) advective term. All terms are averaged by 48 x 48 km blocks and normalized by daily domain-mean $var(\hat{h})$ ($\{\hat{h'}\}$), in units of d-1. Blocks are sorted by h' in ascending order, with dry regions on the left and moist regions on the right. The black solid line is the $\hat{h} = 0$ contour, while dashed horizontal lines represents the genesis time. Values taken from simulation at 301K in 2304 km domain.

8 Reference

Arnold, N. P., and W. M. Putman, 2018: Nonrotating Convective Self-Aggregation in a Limited Area AGCM. *Journal of Advances in Modeling Earth Systems*, **10**, 1029–1046, https://doi.org/10.1002/2017MS001218.

Bretherton, C. S., P. N. Blossey, and M. Khairoutdinov, 2005: An Energy-Balance Analysis of Deep Convective Self-Aggregation above Uniform SST. *Journal of the Atmospheric Sciences*, **62**, 4273–4292, https://doi.org/10.1175/JAS3614.1.

Bryan, G. H., 2012: Effects of Surface Exchange Coefficients and Turbulence Length Scales on the Intensity and Structure of Numerically Simulated Hurricanes. *Monthly Weather Review*, **140**, 1125–1143, https://doi.org/10.1175/MWR-D-11-00231.1.

——, and J. M. Fritsch, 2002: A benchmark simulation for moist nonhydrostatic numerical models. *Mon Weather Rev*, **130**, 2917–2928, https://doi.org/10.1175%2F1520-0493%282002%29130%3C2917%3AABSFMN%3E2.0.CO%3B2.

Carstens, J. D., and A. A. Wing, 2020: Tropical Cyclogenesis From Self-Aggregated Convection in Numerical Simulations of Rotating Radiative-Convective Equilibrium. *Journal of Advances in Modeling Earth Systems*, **12**, https://doi.org/10.1029/2019MS002020.

——, and ——, 2022: A Spectrum of Convective Self-Aggregation Based on Background Rotation. *Journal of Advances in Modeling Earth Systems*, **14**, https://doi.org/10.1029/2021MS002860.

Chavas, D. R., 2013: Tropical Cyclone Size in Observations and in Radiative-Convective Equilibrium. PhD thesis, Massachusetts Institute of Technology, .

——, and K. A. Reed, 2019: Dynamical Aquaplanet Experiments with Uniform Thermal Forcing: System Dynamics and Implications for Tropical Cyclone Genesis and Size. *Journal of the Atmospheric Sciences*, **76**, 2257–2274, https://doi.org/10.1175/JAS-D-19-0001.1.

Clough, S. A., M. W. Shephard, E. J. Mlawer, J. S. Delamere, M. J. Iacono, K. Cady-Pereira, S. Boukabara, and P. D. Brown, 2005: Atmospheric radiative transfer modeling: A summary of the AER codes. *Journal of Quantitative Spectroscopy and Radiative Transfer*, **91**, 233–244, https://doi.org/10.1016/J.JQSRT.2004.05.058.

Coppin, D., and S. Bony, 2015: Physical mechanisms controlling the initiation of convective self-aggregation in a General Circulation Model. *Journal of Advances in Modeling Earth Systems*, **7**, 2060–2078, https://doi.org/10.1002/2015MS000571.

Davis, C. A., 2015: The Formation of Moist Vortices and Tropical Cyclones in Idealized Simulations. *Journal of the Atmospheric Sciences*, **72**, 3499–3516, https://doi.org/10.1175/JAS-D-15-0027.1.

Donelan, M. A., B. K. Haus, N. Reul, W. J. Plant, M. Stiassnie, H. C. Graber, O. B. Brown, and E. S. Saltzman, 2004: On the limiting aerodynamic roughness of the ocean in very strong winds. https://doi.org/10.1029/2004GL019460.

Drennan, W. M., J. A. Zhang, J. R. French, C. McCormick, and P. G. Black, 2007: Turbulent Fluxes in the Hurricane Boundary Layer. Part II: Latent Heat Flux. *Journal of the Atmospheric Sciences*, **64**, 1103–1115, https://doi.org/10.1175/JAS3889.1.

Emanuel, K. A., 1986: An Air-Sea Interaction Theory for Tropical Cyclones. Part I: Steady-State Maintenance. *Journal of the Atmospheric Sciences*, **43**, 585–604.

——, 1987: The dependence of hurricane intensity on climate. *Nature 1987 326:6112*, **326**, 483–485, https://doi.org/10.1038/326483a0.

——, 2012: Self-Stratification of Tropical Cyclone Outflow. Part II: Implications for Storm Intensification. *Journal of the Atmospheric Sciences*, **69**, 988–996, https://doi.org/10.1175/JAS-D-11-0177.1.

——, A. A. Wing, and E. M. Vincent, 2014: Radiative-convective instability. *Journal of Advances in Modeling Earth Systems*, **6**, 75–90, https://doi.org/10.1002/2013MS000270.

Fairall, C. W., E. F. Bradley, J. E. Hare, A. A. Grachev, and J. B. Edson, 2003: Bulk Parameterization of Air-Sea Fluxes: Updates and Verification for the COARE Algorithm. *American Meteorological Society*, **16**, 571–591, https://doi.org/10.2307/26249616.

Gray, W. M., 1968: Global View of the Origin of Tropical Disturbances and Storms. *Mon. Wea. Rev.*, 669–700.

——, 1977: Tropical Cyclone Genesis in the Western North Pacific. *Journal of the Meteorological Society of Japan. Ser. II*, **55**, 465–482, https://doi.org/10.2151/JMSJ1965.55.5_465.

Held, I. M., and M. Zhao, 2008: Horizontally Homogeneous Rotating Radiative–Convective Equilibria at GCM Resolution. *Journal of the Atmospheric Sciences*, **65**, 2003–2013, https://doi.org/10.1175/2007JAS2604.1.

Holloway, C. E., and S. J. Woolnough, 2016: The sensitivity of convective aggregation to diabatic processes in idealized radiative-convective equilibrium simulations. *Journal of*

Advances in Modeling Earth Systems, **8**, 166–195, https://doi.org/10.1002/2015MS000511.

Iacono, M. J., J. S. Delamere, E. J. Mlawer, M. W. Shephard, S. A. Clough, and W. D. Collins, 2008: Radiative forcing by long-lived greenhouse gases: Calculations with the AER radiative transfer models. *Journal of Geophysical Research: Atmospheres*, **113**, 13103, https://doi.org/10.1029/2008JD009944.

Khairoutdinov, M. F., and K. A. Emanuel, 2010: Aggregated Convection and the Regulation of Tropical Climate. *paper presented at 29th Conference on Hurricanes and Tropical Meteorology, Am. Meteorol. Soc., Tucson, Ariz.*, https://doi.org/10.1029/2009GL039667.

——, and K. Emanuel, 2013: Rotating radiative-convective equilibrium simulated by a cloud-resolving model. *Journal of Advances in Modeling Earth Systems*, **5**, 816–825, https://doi.org/10.1002/2013MS000253.

Knutson, T. R., and Coauthors, 2010: Tropical cyclones and climate change. *Nature Geoscience 2010 3:3*, **3**, 157–163, https://doi.org/10.1038/ngeo779.

Mlawer, E. J., S. J. Taubman, P. D. Brown, M. J. Iacono, and S. A. Clough, 1997: Radiative transfer for inhomogeneous atmospheres: RRTM, a validated correlated-k model for the longwave. *Journal of Geophysical Research: Atmospheres*, **102**, 16663–16682, https://doi.org/10.1029/97JD00237.

Mol, W. B., C. C. van Heerwaarden, and L. Schlemmer, 2019: Surface Moisture Exchange Under Vanishing Wind in Simulations of Idealized Tropical Convection. *Geophysical Research Letters*, **46**, 13602–13609, https://doi.org/10.1029/2019GL085047.

Morrison, H., J. A. Curry, and V. I. Khvorostyanov, 2005: A New Double-Moment Microphysics Parameterization for Application in Cloud and Climate Models. Part I: Description. *Journal of the Atmospheric Sciences*, **62**, 1665–1677, https://doi.org/10.1175/JAS3446.1.

——, G. Thompson, and V. Tatarskii, 2009: Impact of Cloud Microphysics on the Development of Trailing Stratiform Precipitation in a Simulated Squall Line: Comparison of One- and Two-Moment Schemes. *Monthly Weather Review*, **137**, 991–1007, https://doi.org/10.1175/2008MWR2556.1.

Muller, C. J., and I. M. Held, 2012: Detailed Investigation of the Self-Aggregation of Convection in Cloud-Resolving Simulations. *Journal of the Atmospheric Sciences*, **69**, 2551–2565, https://doi.org/10.1175/JAS-D-11-0257.1.

——, and D. M. Romps, 2018: Acceleration of tropical cyclogenesis by self-aggregation feedbacks. *Proc Natl Acad Sci U S A*, **115**, 2930–2935, https://doi.org/10.1073/PNAS.1719967115/-/DCSUPPLEMENTAL.

Murthy, V. S., and W. R. Boos, 2018: Role of Surface Enthalpy Fluxes in Idealized Simulations of Tropical Depression Spinup. *Journal of the Atmospheric Sciences*, **75**, 1811–1831, https://doi.org/10.1175/JAS-D-17-0119.1.

National Hurricane Center and Central Pacific Hurricane Center, N., Tropical Cyclone Climatology. https://www.nhc.noaa.gov/climo/index.php (Accessed August 15, 2022).

Naumann, A. K., B. Stevens, C. Hohenegger, and J. P. Mellado, 2017: A Conceptual Model of a Shallow Circulation Induced by Prescribed Low-Level Radiative Cooling. *Journal of the Atmospheric Sciences*, **74**, 3129–3144, https://doi.org/10.1175/JAS-D-17-0030.1.

Nolan, D. S., 2007: What is the trigger for tropical cyclogenesis? *Australian Meteorological Magazine*, **56**, 241–266.

——, E. D. Rappin, and K. A. Emanuel, 2007: Tropical cyclogenesis sensitivity to environmental parameters in radiative-convective equilibrium. *Quarterly Journal of the Royal Meteorological Society*, **133**, 2085–2107, https://doi.org/10.1002/QJ.170.

Palmen, E. H., 1948: On the formation and structure of tropical cyclones. *Geophysica*, **3**, 26–38.

Pope, K. N., C. E. Holloway, T. R. Jones, and T. H. M. Stein, 2021: Cloud-Radiation Interactions and Their Contributions to Convective Self-Aggregation. *Journal of Advances in Modeling Earth Systems*, **13**, e2021MS002535, https://doi.org/10.1029/2021MS002535.

Ramsay, H. A., M. S. Singh, and D. R. Chavas, 2020: Response of Tropical Cyclone Formation and Intensification Rates to Climate Warming in Idealized Simulations. *Journal of Advances in Modeling Earth Systems*, **12**, e2020MS002086, https://doi.org/10.1029/2020MS002086.

Riehl, H., 1950: A Model of Hurricane Formation. *Journal of Applied Physics*, **21**, 917, https://doi.org/10.1063/1.1699784.

Rotunno, R., and A. Emanuel, 1987: An air-sea interaction theory for tropical cyclones. Part II: Evolutionary study using a nonhydrostatic axisymmetric numerical model. *Journal of the Atmospheric Sciences*, 542–561, https://doi.org/10.1175/1520-0469(1987)044.

Ruppert, J. H., A. A. Wing, X. Tang, and E. L. Duran, 2020: The critical role of cloud–infrared radiation feedback in tropical cyclone development. *Proc Natl Acad Sci U S A*, **117**, 27884–27892, https://doi.org/10.1073/PNAS.2013584117/-/DCSUPPLEMENTAL.

Wang, Y., C. A. Davis, and Y. Huang, 2019: Dynamics of Lower-Tropospheric Vorticity in Idealized Simulations of Tropical Cyclone Formation. *Journal of the Atmospheric Sciences*, **76**, 707–727, https://doi.org/10.1175/JAS-D-18-0219.1.

Wing, A. A., 2022: Acceleration of tropical cyclone development by cloud-radiative feedbacks. *Journal of the Atmospheric Sciences*, **1**, https://doi.org/10.1175/JAS-D-21-0227.1.

——, and K. A. Emanuel, 2014: Physical mechanisms controlling self-aggregation of convection in idealized numerical modeling simulations. *J Adv Model Earth Syst*, **6**, 59–74, https://doi.org/10.1002%2F2013MS000269.

——, and T. W. Cronin, 2016: Self-aggregation of convection in long channel geometry. *Quarterly Journal of the Royal Meteorological Society*, **142**, 1–15, https://doi.org/10.1002/QJ.2628.

——, S. J. Camargo, and A. H. Sobel, 2016: Role of Radiative–Convective Feedbacks in Spontaneous Tropical Cyclogenesis in Idealized Numerical Simulations. *Journal of the Atmospheric Sciences*, **73**, 2633–2642, https://doi.org/10.1175/JAS-D-15-0380.1.

——, K. Emanuel, H. E. Christopher, and C. Muller, 2017: Convective Self-Aggregation in Numerical Simulations: A Review. *Surveys in Geophysics*, **38**, 1173–1197, https://doi.org/10.1007/s10712-017-9408-4.

——, K. A. Reed, M. Satoh, B. Stevens, S. Bony, and T. Ohno, 2018: Radiative-convective equilibrium model intercomparison project. *Geosci. Model Dev*, **11**, 793–813, https://doi.org/10.5194/gmd-11-793-2018.

——, and Coauthors, 2020: Clouds and Convective Self-Aggregation in a Multimodel Ensemble of Radiative-Convective Equilibrium Simulations. *Journal of Advances in Modeling Earth Systems*, **12**, e2020MS002138, https://doi.org/10.1029/2020MS002138.

Zhang, F., and K. Emanuel, 2016: On the Role of Surface Fluxes and WISHE in Tropical Cyclone Intensification. *Journal of the Atmospheric Sciences*, **73**, 2011–2019, https://doi.org/10.1175/JAS-D-16-0011.1.